Diffusion and Catalytic Cracking of 1,3,5 Tri-iso-propyl-benzene in FCC Catalysts

S.Al-Khattaf[1] , J. A. Atias[2], K.Jarosch [3], H.de Lasa[3*]
(1) Chemical Engineering Department, King Fahd University of Petroleum and Minerals,Dhahran, 31261 Saudi Arabia.
(2) Departamento de Termodinámica y Fenómenos de Transferencia. Universidad Simón Bolívar, Caracas, Venezuela.
(3) Chemical Reactor Engineering Centre, Faculty of Engineering, University of Western Ontario, London, Ontario, Canada N6A 5B9.

Abstract

The present study describes catalytic cracking experiments developed in a novel CREC Riser Simulator using 1,3,5-Tri-iso-propyl-benzene and two FCC catalysts with different crystal sizes (0.4-μm and 0.9-μm diameter). The experiments are modeled using an unsteady state model for both gas and catalyst phases. It is found that a quasi-steady state approximation can be used for the catalyst and changes in the gas phase can be accounted, under the allowed model simplifications, with a relatively simple unsteady state equation. The model is completed using two catalytic decay models, with one of them involving a decay function based on "reactant converted". Experimental and modeling observations point towards an overall cracking reaction rate controlled by diffusion at 350°C – 450°C with this rate shifting to one being controlled by the intrinsic cracking reaction at 500°C – 550°C.

(*) Author to whom correspondence may be addressed

1-Introduction

The oil refining industry has experienced in recent years, a dramatic increase in the price and availability of crude oil. In this respect, new catalyst technology is needed to process heavier feedstocks and to produce more environmentally friendly products.

The currently available 60-μm commercial FCC catalysts are manufactured with 1-2-μm Y-zeolite crystals dispersed in an amorphous silica-alumina matrix (Venuto and Habib, 1979). The majority of the active sites are located within the zeolite pore structure. In order for the reaction to proceed, molecules have to diffuse through the large matrix pores into the zeolite crystals. As a result, only certain hydrocarbon species with a kinetic diameter smaller than 10.2 Å can penetrate the zeolite pores (Leiby, 1992). Hence the relationship between catalytic cracking reaction and diffusional processes can determine the extent of cracking and greatly influence the product selectivity. Such phenomena are complex and theoretical models to describe such systems are needed (Bidabehere and Sedran, 2000).

Diffusion in catalysts belongs in many cases to the Knudsen regime. However, diffusion in zeolites falls more in a so-called "configurational regime", since the size of the hydrocarbon molecule is nearly the size of the zeolite inner channels (Karger and Ruthven, 1992; Gates et al,1979). As a result, diffusion of the hydrocarbon molecules is governed by an almost continuous interaction between the zeolite crystal and the diffusing molecules (Karger and Ruthven,1992;Gates et al,1979). In addition, there may be compounded effects

with larger hydrocarbon molecules hindering the diffusion of smaller molecules. As a result, lighter product molecules may be trapped or delayed in a zeolite pore network already filled with sorbed heavier molecules (Gates et al, 1979).

The 1,3,5-TIPB is a relatively bulky molecule with a critical molecular diameter of about 9.5 Å (Bhatai, 1991). Due to its large size, it has been used to simulate the diffusional constrains expected in the catalytic cracking of gas oil (Aguiar et al, 1995). For instance, the cracking of 1,3,5-TIPB was used to study the effect of Y-zeolite external surface on 1,3,5-TIPB conversion using two Y-zeolite with different crystal sizes. In this respect, Aguiar et al (1995), pointed out that small zeolite crystals (0.8-μm) have, at 370°C, a higher 1,3,5-TIPB conversion than the larger zeolite crystals (1.6-μm). These authors inferred that this behavior was due to the change of zeolite external surface area. Even if this study represents one of the first contributions regarding effects of crystal size on 1,3,5-TIPB conversion, the effect of zeolite size on selectivity was not investigated. Roos et al (1997) reported that different zeolitic materials might provide catalysts for the 1,3,5-TIPB cracking, with different activity and selectivity. It was shown that MCM-41 catalyst with extra large pore shows the highest conversion. The activity of this catalyst was followed by the commercial FCC catalyst (active matrix precracking), HY-zeolite, and finally Si-VPI-5 which has the smallest pores. Thus, based on these studies, it can be speculated that the size of the zeolite crystal and the opening of the pores can have a very important role determining the reaction pathway of large molecules, case of 1,3,5-TIPB.

To clarify these matters and to further progress on the modeling of diffusional effects, data from the CREC Riser Simulator, a novel unit invented by de Lasa (1991) which overcomes the technical problems of the standard micro-activity test (MAT), are considered.

2- Modeling the 1,3,5-TIPB Catalytic Cracking. Unsteady State Reaction Model

FCC catalysts are manufactured with pellets of close to 60-μm. Zeolite particles are dispersed, as illustrated in Figure 1, in the catalyst matrix. The faujasite-type zeolites give important reaction and adsorption properties to the FCC catalyst. In addition, the large pores of the matrix provide access to the smaller pore network of the Y zeolite crystals. It is expected that adsorption and transport of reactant molecules in this fine zeolite pore structure may control the overall reaction rate and in many cases influence the reaction selectivity.

Catalytic cracking of model components, as considered in the present study, using the CREC Riser Simulator, can be considered as an unsteady state process as follows:

$$-\frac{V}{W_{cr}}\frac{dC^{*}_{A,ex}}{dt}=\left\{D_{eff}\left.\frac{\partial C^{*}_{A,in}}{\partial r}\right|_{r=R_{cr}}\right\}\frac{3}{R_{cr}\rho_{cr}} \qquad (1)$$

with $C^{*}_{A,ex} = \frac{C_{A,ex}}{C_{A,ex}\big|_{\tau=0}}$ representing the 1,3,5-TIPB dimensionless concentration outside the crystal and $C^{*}_{A,in} = \frac{C_{A,in}}{C_{A,ex}\big|_{\tau=0}}$ representing the 1,3,5-TIPB dimensionless concentration in the crystal.

The above equation hypothesizes that both adsorption and reaction phenomena take place in the zeolite crystals only, with the catalyst matrix being inert to the adsorption-reaction processes. Thus, modeling of the cracking reaction, as given in eq. (1) has to be complemented by the solution of a partial differential equation in the zeolite crystals as follows,

$$\frac{1}{r^{*2}}\frac{\partial}{\partial r^{*}}\left(r^{*2}\frac{\partial C^{*}_{A,in}}{\partial r^{*}}\right) = h^{2}C^{*}_{A,in} + \frac{\partial C^{*}_{A,in}}{\partial \tau} \qquad (2)$$

where $h = R_{cr}\sqrt{\frac{k_{A,in}\varphi_{in}\rho_{cr}}{D_{eff}}}$ is the Thiele modulus, a non-dimensional group that compares the reaction rate to the diffusion rate, $\tau = \frac{D_{eff}t}{R_{cr}^{2}(\varepsilon + K\rho_{cr})}$ a dimensionless time and $r^{*} = \frac{r}{R_{cr}}$ a dimensionless radial position.

Eqs. (1) and (2) are applicable for modeling catalytic cracking of 1,3,5-TIPB given that, in a CREC Riser Simulator unit, the following applies: a) quasi-isothermal conditions, b) batch operation, c) intense recirculation of chemical species, d) dominant fluidized bed conditions.

In addition, modeling catalytic cracking in the Riser Simulator requires a number of initial and boundary conditions which consider instantaneous vaporization ($t = 0$, $C_{A,ex} = C_{A,ex}\big|_{t=0}$), symmetric concentration profiles inside the

crystals ($r = 0$, $\partial C_{A,in} / \partial r = 0$), negligible transport limitations around the 60 μm particles and inside the matrix ($r = R_c$, $C_{A,in} = C_{A,ex}$).

Reviewing eq. (2) it can be observed that changes of concentration in the crystals are going to be affected by the two right hand side terms in this equation: a) a reaction term, b) an accumulation/deaccumulation term. The relative importance of these two terms may change with the extent of reaction, with the accumulation term, being more dominant at the beginning of the reaction and becoming essentially negligible after a given reaction time. Under these conditions, as it will be described later, the operation of an FCC catalyst, in the CREC Riser Simulator, can be viewed as: a) an unsteady process, in the bulk gas phase of the reactor, and b) a quasi-steady state process, inside the zeolite crystals.

To assess this, and the conditions where the accumulation term of eq. (2) is negligible, eqs. (1) and (2) were solved numerically using finite difference equations. Table 1 reports the parameters and conditions employed in this calculation. Regarding these conditions (T=350°C, catalyst/hydrocarbon=5 g/g, zeolite crystal size =0.9-μm or CAT-LC), they were selected given they represent a worst scenario case, regarding the influence of the accumulation term in eq (2). Figure 2 reports the results of this calculation. The adequacy of this simplification is also reported in Figures 3a and 3b where the effectiveness factor is calculated at various reaction times, using the calculated concentration profiles:

$$\eta = \frac{r_{mean}}{k_{A,in} C_{A,in}\big|_{r=R_{cr}}} = \frac{3\int_0^1 C^*_{A,in} r^{*2} dr^*}{C^*_{A,ex}} \qquad (3)$$

The effectiveness factor increases in a progressive manner, becoming essentially after 1-sec. the effectiveness factor at steady state (η_{ss}). Deviations between the η and the η_{ss} at 350C and 1–sec., fall below 1.5%. Thus, the contribution of the unsteady state term in eq. (2) may be important for reaction times between 0 and 0.5-sec only. Following this, the dimensionless concentration profile inside the crystals is essentially independent of accumulation effects.

Given that all data in the CREC Riser Simulator, as it will be described in the upcoming sections, was taken at 3, 5, 7 and 10-sec. and that the simulation of Figs. 2, 3a and 3b represent a worst scenario case, the "quasi-steady state" assumption for eq. (2) can be considered adequate.

3- Modeling the Catalytic Cracking of 1,3,5-TIPB. Quasi-steady state approximation.

Given the discussion and considerations of the previous section, modeling catalytic cracking of 1,3,5-TIPB, in the CREC Riser Simulator, becomes essentially the consideration of the following equation with $C_{A,ex}$ becoming the C_A concentration:

$$-\frac{V}{W_{cr}}\frac{dC_A}{dt} = \eta_{ss} r_A \qquad (4)$$

Moreover, in order to further progress in the analysis one has to postulate catalyst activity decay functions and adequate approaches to calculate η_{ss}.

(i)-Catalyst Activity Decay Function Based on Reactant Conversion (RC).

A catalyst activity decay function can be conveniently expressed as a function of the reactant converted. This approach can be represented as follows:

$$-\frac{V}{W_{cr}}\frac{dC_A}{dt} = \eta_{ss} k_{A,in} \varphi_{in} C_A \tag{5}$$

where C_A is the 1,3,5-TIPB concentration at any reaction time.

Moreover, C_A can be related to y_A as,

$$C_A = \frac{y_A W_{hc}}{MW_A V} \tag{6}$$

Then eq. (1) can be written in terms of the y_A molar fraction,

$$-\frac{V}{W_{cr}}\frac{dy_A}{dt} = \eta_{ss} k_{A,in} \varphi_{in} y_A \tag{7}$$

Given that coke formation can be postulated to take place as proportion of hydrocarbon conversion, with coke being "mainly" the result of the primary cracking reaction steps. Then,

$$\frac{dX_{coke}}{dy_A} = -\nu_{coke}\frac{W_{hc}}{W_{cr}}\frac{MW_{coke}}{MW_A} \tag{8}$$

Since the right side of eq. (8) can be assumed as constant parameter, then eq. (8) can be written as,

$$\frac{dX_{coke}}{dy_A} = A \tag{9}$$

where A lumps a group of parameters.

By integrating eq. (9) between 0 and X_{coke} and between 1 and y_A, the following equation is obtained,

$$X_{coke} = A(1 - y_A) \tag{10}$$

with

$$A = -\frac{\nu_{coke} W_{hc} MW_{coke}}{W_{cr} MW_A} \tag{11}$$

where X_{coke} is the coke mass fraction based on the catalyst weight.

Once the conversion of reactant to the coke fraction is established, the following step in the analysis is to consider a catalyst activity decay function based on coke concentration, as proposed by Froment (1979):

$$\varphi_{in} = \exp(-\delta X_{coke}) \tag{12}$$

However, given the relationship between the coke concentration on catalyst, X_c and the weight fraction of 1,3,5-TIPB, y_A, as given by eq. (10), the following equation results,

$$\varphi_{int} = \exp(-\lambda(1-y_A)) \tag{13}$$

where

$$\lambda = A\delta \tag{14}$$

Substituting eqs. (13) in eq. (7) it results:

$$-\frac{V}{W_{cr}}\frac{dy_A}{dt} = \eta_{ss} k_0^{'} \exp\left[\frac{-E_R}{R}\left(\frac{1}{T}-\frac{1}{T_0}\right)\right]\exp(-\lambda(1-y_A))y_A \tag{15}$$

This model, so called "reactant conversion" model (RC) was also successfully tested, for the catalytic cracking of cumene (Al-Khattaf and de Lasa, 2001a; Al-Khattaf, 2001).

(ii)-Catalyst Activity Decay Function Based on time-on-stream (TOS).

The catalyst activity decay model based on time-on-stream was initially suggested by Voorhies (1945). Since then, this model has been used extensively throughout the FCC literature. This model is empirically based given it does not incorporate a mechanistic description of catalyst deactivation. As a result, extrapolations of activity decay with this model are quite uncertain.

Thus, considering eq. (4), the changes of 1,3,5-TIPB concentrations can be represented as,

$$-\frac{V}{W_c}\frac{dy_A}{dt}=\eta_{ss}k_0^{'}\exp\left[\frac{-E_R}{R}\left(\frac{1}{T}-\frac{1}{T_0}\right)\right]\varphi_{in}y_A \tag{16}$$

Based on the time-on-stream model, φ_{in} can be expressed as

$$\varphi_{in}=\exp(-\alpha t) \tag{17}$$

and the changes of 1,3,5-TIPB are given as follows,

$$-\frac{V}{W_c}\frac{dy_A}{dt}=\eta_{ss}k_0^{'}\exp\left[-\frac{E_R}{R}\left(\frac{1}{T}-\frac{1}{T_0}\right)\right]\exp(-\alpha t)y_A \tag{18}$$

(iii)-The effectiveness factor of 1,3,5-TIPB catalytic cracking

The effectiveness factor is a dimensionless quantity expressing the extent of diffusional constrains inside a catalyst. The effectiveness factor for a zeolite crystal under steady state conditions (η_{ss}) is defined as the ratio of the actual reaction rate to the reaction rate in the absence of the internal diffusional resistance (Smith,1981; Aris,1969).

$$\eta_{ss}\approx\frac{\tanh(h')}{h'} \tag{19}$$

The effectiveness factor, η_{ss}, requires the definition of a modified Thiele modulus, h'. This modified Thiele modulus, h', depends on the zeolite size, the zeolite crystal geometry, the zeolite crystal apparent density, the reactant diffusivity and the intrinsic rate constant as follows:

$$h'=\frac{1}{a_{ext}}\sqrt{\frac{k_{A,in}\rho_{cr}\varphi_{in}}{D_{eff}}} \tag{20}$$

with a_{ext} being the specific external surface area for the zeolite crystal (a_{ext} = $3/R_{cr}$), D_{eff} the effective diffusivity φ_{in} the intrinsic catalyst activity decay function and $k_{A,in}$ the intrinsic kinetic constant for the 1,3,5-TIPB at time t=0.

Moreover, the effective diffusivity coefficient in zeolites can be represented using the Eyring equation (Karger and Ruthven, 1992) centering the definition of D in To, a reference temperature of 450°C,

$$D_{eff}=D_0 \exp\left(-\frac{E_D}{R}\left[\frac{1}{T}-\frac{1}{T_o}\right]\right) \tag{21}$$

where E_D represents the diffusion activation energy.

Eq. (21) is a useful relationship to estimate the effect of temperature on the 1,3,5-TIPB transport. Based on the experimental data reported by Ruthven and Kaul (1993) on the diffusivity of 1,3,5 TEB in faujasite zeolite, with a critical diameter of 9Å, E_D was estimated at 17 kcal/mole (Ruthven and Kaul, 1993; Karger and Ruthven, 1992). Since 1,3,5-TIPB and 1,3,5-TEB have close critical molecular diameter, it is expected that E_D for 1,3,5-TIPB should be in a close range. Considering the initial conversion rates, observed in the present study for both CAT-LC and CAT-LC, at h'=1, a similar energy of activation of 16 kcal/mole and a D_o=0.2.10-12 m^2/s were estimated. These E_D and D_o values were employed in subsequent calculations of the effectiveness factor (η_{ss}), substituting eq. (21) in eq. (20) and using the resulting h' in eq (19).

3- Experimental Procedures

1,3,5 tri-iso-propyl-benzene (1,3,5-TIPB) (Fluka 92075) was employed as model reactant compound. Regarding the FCC catalysts, commercially available

Y-zeolites (small and large crystals) from Tosoh Company were used. Properties of these zeolites are reported in Table 2.

These Na-zeolites were ion exchanged with NH_4NO_3 to replace the sodium cation with the NH_4^+ cation. Following this, NH_3 was removed and the H form of the zeolites was spray-dried using kaolin, as the filler, and silica sol, as the binder. The resulting 60-μm catalyst particles had the following composition: 30 wt% zeolite, 50 wt% kaoline, and 20 wt% silica sol. The process of sodium removal was repeated for the pelletized catalyst. Following this, the catalyst was calcined during 2 hr at 600°C. Finally, the fluidizable catalyst particles (60-μm average size) were treated with 100% steam at 760°C for 5 hr. Table 3 reports the catalyst main properties following catalyst pretreatment. The unit cell size was determined by X-ray diffraction following ASTM D-3942-80. Surface area was measured using the BET method. It can be observed that, for both zeoltes, the initial zeolite unit cell size of 24.5 Å was reduced, following steaming treatment, to around 24.28Å.

4-Reaction Evaluation

The catalytic activity of the Y-zeolite catalyst, prepared using the various techniques described above, was measured in a 48 cm^3 CREC Riser Simulator using 1,3,5 tri-iso-propyl-benzene (1,3,5-TIPB). The Riser Simulator is a novel bench scale, invented by de Lasa (1992). This unit overcomes the technical problems of the standard micro-activity test (MAT) and is becoming a most valuable experimental tool for testing and developing new FCC catalysts (Arandes et al, 2000; Arandes et al, 1997; Bidabehere and Sedran, 2000; Sedran, 1994).

A schematic diagram of the Riser Simulator is reported in Figure 4. The Riser Simulator consists of two outer shells, lower section and upper section that permits to load or to unload the catalyst easily. This reactor was designed in such way that an annular space is created between the outer portion of the basket and the inner part of the reactor shell. A metallic gasket seals the two chambers, an impeller located in the upper section. A packing gland assembly and a cooling jacket surrounds the shaft supports the impeller. Upon rotation of the shaft, gas is forced outward from the center of the impeller towards the walls. This creates a lower pressure in the center region of the impeller thus, inducing flow of gas upward through the catalyst chamber from the bottom of the reactor annular region where the pressure is slightly higher. The impeller provides a fluidized bed of catalyst particles as well as intense gas mixing inside the reactor.

The Riser Simulator operates in conjunction with a series of sampling valves that allow (Figure 5), following a predetermined sequence, to inject hydrocarbons and withdraw products in short periods of time. A Hewlett Packard 5890A GC allows the quantification of reaction products using an FID detector and a capillary column HP-1, 25 m cross-linked methyl silicone with an outer diameter of 0.22 mm and an internal diameter of 0.33 microns. A more detailed description of various components of the Riser Simulator and the sequence of injection and sampling can be found in Pruski (1996).

5-Experimental Results and Evaluation of Model Parameters

The 1,3,5-TIPB is a valuable model compound to study diffusion and reaction in FCC catalysts. The advantages of using this model compound can be

summarized as follows; a) It can be considered a typical gas oil molecule, b) It has 9.5Å critical diameter significantly larger than the 7.4Å Y-zeolite opening, c) The reaction path is relatively easy to follow since alkylbenzenes crack following a reported mechanism (Fig. 6).

Figures 7 and 8 report the 1,3,5-TIPB conversions at C/O=5 and for several temperatures (400°C, 450°C, 500°C, 525°C, 550°C) and reaction times (3-sec. and 5-sec.). It was observed that for both catalysts (CAT-LC and CAT-SC) and for all the temperatures studied, the 1,3,5-TIPB conversion increases with reaction time (3-10 sec.). This is an expected behavior given that at longer residence times there is an increased opportunity of the 1,3,5-TIPB hydrocarbon molecules to be cracked. This trend is, however, moderated at longer residence times and this is due to coke formation.

The effect of the temperature on the 1,3,5-TIPB conversion is also reported in Figures 7 and 8 for C/O=5, 3-sec. and 5-sec. It can be noticed that increasing the temperature, for a set reaction time, the conversion augments up to a given level. From this temperature and on, there is no significant influence on the 1,3,5-TIPB conversion. For instance, for the CAT-LC catalyst the 1,3,5-TIPB conversion increases with temperature until it almost stabilizes at 525°C. Any further increases in temperature do not have a major influence on the 1,3,5-TIPB conversion. On the other hand the CAT-SC catalyst displays a similar behavior at 500°C. For instance, at 5-sec. (Figure 8), the conversion is around 47% for 500°C and 49% for 550°C with these conversions staying at similar levels for higher temperatures. It has to be stressed that this type of influence of temperature in

the 1,3,5-TIPB conversion was observed for the different reaction times of 3, 5, 7 and 10-sec. studied.

Regarding the various steps involved in the catalytic cracking of 1,3,5-TIPB, a network of three prevailing in-series reactions can be considered (Figure 6): a) 1,3,5-TIPB de-alkylation yields 1,3-DIPB and propylene, b) 1,3-DIPB dealkylation gives cumene and propene, c) cumene de-alkylation forms benzene and propene (Al-Khattaf and de Lasa, 2001b). While the above-mentioned steps are the dominant ones, there are other reactions such as disproprotionation, isomerization and condensation (Corma and Wojciechowski, 1982) that may affect gas phase product distribution and coke formation. The extent of these steps may depend on both temperature and catalyst properties (Tsai et al., 1999).

Thus, given the nature of the 1,3,5-TIPB cracking reaction it is important to examine product selectivity and the influence of both operating conditions and crystal size on product selectivity. For instance, in a recent study Al-Khattaf and de Lasa (2001a), it was observed that the 1,3-DIPB selectivity, is mainly the result of the first dealkylation step, which importance increases with time and decreases with both temperature and crystal size. It should also noticed that cumene selectivity was always much higher than 1,3 DIPB selectivities (almost 5 times). This was assigned to the higher crackability of the 1,3-DIPB molecule versus the cumene molecule.

(i) Decay model based on time-on-stream (TOS).

Using the data from different 1,3,5-TIPB cracking runs, the three model parameters of eq. (18) where adjusted using non-linear regression (Table 4). The

resulting cross-correlation matrix is reported, for both catalysts, in Tables 4 and 5. It was observed that a 0.955 kcal/mole energy of activation (E_R) was obtained for 1,3,5-TIPB cracking using CAT-LC. A close value of 2.64 kcal/mole was obtained for CAT-SC. The determined set of parameters, obtained with this calculation, represent intrinsic kinetic constants of both cracking and activity decay. These intrinsic kinetic constants were determined with restricted 95% confident limits and limited parameter cross-correlation.

Given that the value for the E_D, activation energy for the 1,3,5-TIPB in Y zeolites, as assessed in the present study, is 16 kcal/mole and considering that the activation energies for the intrinsic catalytic cracking reaction (refer to Table 4), one can estimate for the diffusional controlled regime an apparent activation energy $E_{app}= (E_D+E_R)/2$ of 8.45 and 9.32 Kcal/mole for the CAT-LC and CAT-LC respectively.

A reconciliation plot showing the good agreement between experimental conversions and model predictions are also reported in Figs 9a and 9b for CAT-LC and CAT-SC respectively.

(ii) Decay model based on reactant conversion (RC).

The same set of catalytic cracking runs developed with 1,3,5-TIPB were modeled using the more mechanistically sound eq. (15), an activity decay function based on the reactant conversion model. In this case, the differential eq. (15) was solved and the three model parameters (k'_o, E_R, λ) were adjusted simultaneously using non-linear regression.

The RC decay model gave for the CAT-LC an activation energy of 6.19 kcal/mole and an activity decay constant (λ) of 3.69 (Table 6). Close values of 7.19 Kcal/mol activation energy and 3.84 decay constant were obtained for CAT-SC. It should be mentioned that in both cases the 95% confident limit was restricted with limited parameter cross-correlation (Tables 8 and 9). Reconciliation plots between the experimental results and the model predictions are also reported in Figs. 10a and 10b showing adequate fitting for CAT-LC and CAT-SC. Model predictions based on RC model are reported in Figs 11 and Fig 12.

Regarding the kinetic parameters obtained, it should be specifically mentioned that these parameters represent intrinsic reaction constants. The fact that both catalysts display very similar intrinsic parameters is particularly encouraging given the close chemical composition and pretreatment of CAT-LC and CAT-SC.

Furthermore, to check the suitability of eq. (10) for the 1,3,5-TIPB cracking, independent experiments were developed. The experiments involved the simultaneous determination of coke and 1,3,5-TIPB conversion. Figures 13 and 14 demonstrate that for both low temperature and high temperature range, the coke selectivity or eq. (10) is not a function of reaction time. Furthermore, it can also be stated that the A parameter is a weak function of temperature. Generally the A parameter oscillates between 0.5% (for T=400°C) and 0.35% (for T=550°C). Consequently, it can be assumed that coke selectivity of 1,3,5-TIPB cracking, at a set C/O and temperature range, is independent of the reaction conditions.

5-The η_{ss} effectiveness factor

Regarding the η_{ss} effectiveness factor for 1,3,5-TIPB cracking, it can be calculated using an intrinsic deactivation function, φ_{in}. This intrinsic decay function can be based either on a TOS model or a RC model. In the following sections, both activity decay functions will be used in order to evaluate the effectiveness factor η_{ss}.

In this respect, a first possible calculation of the Thiele modulus (eq. 20) and η_{ss} (eq. 19) can be developed using the α deactivation constant and kinetic parameters obtained from the TOS model (Table 4). Figs 15, 16 and 17 display the changes of η_{ss} with the modified Thiele modulus, h' for both CAT-SC and CAT-LC. All experimental conditions reported are in the 3-10 seconds reaction time and in the 350-550°C temperature range. Figure 15 shows that 1,3,5-TIPB cracking is diffusionally controlled at 350°C, where η_{ss} display values much smaller than one. Figure 15 also reports the increase of η_{ss} with reaction time. This consistent increase of η_{ss} for both catalysts is the result of the effect of the reaction time on the activity decay function reducing the modified Thiele modulus, h', and increasing in turn the effectiveness factor, η_{ss}. In this respect, Figure 15 shows that overall the CAT-SC is subject to smaller intra-crystal diffusional constrains than the CAT-LC and this given the initial η_{ss} values, at 3-sec., are 0.251 and 0.66

for CAT-LC and CAT-SC respectively. These values increase consistently for both catalysts reaching at 10-sec., the values of 0.49 and 0.89 for CAT-LC and CAT-SC respectively.

Intracrystal diffusional constrains were also observed at higher temperature (400°C and 450°C). At 400°C and 3-sec. reaction time, the CAT-LC shows a η_{ss} = 0.401 while the CAT-SC a η_{ss} =0.805. Again here, the η_{ss} for both catalysts augmented with reaction time. Moreover, when these η_{ss} values, obtained at 400 °C, are compared with those observed at 350°C it can be observed that the η_{ss} at 400°C are closer to unity than the η_{ss} values at 350°C. Even more, this trend repeats at 450°C (Fig. 16) with η_{ss} , at 3-sec., of 0.569 and 0.889 for CAT-LC and CAT-SC respectively, yielding η_{ss} which are ordered with temperature as follows:

$$\eta_{ss}\big|_{T=350°C} < \eta_{ss}\big|_{T=400°C} < \eta_{ss}\big|_{T=450°C} < 1 \qquad (22)$$

Given these results it can be argued that diffusional constrains decrease progressively whith temperature and this yields a reduced intracrystaline transport limitations at the higher thermal levels.

Furthermore, when the reaction temperature reached 500°C, η_{ss} values were close to one: a) at 7-sec., η_{ss}=0.972 for CAT-SC and 0.846 for CAT-LC, b) at 10- sec., η_{ss}=0.985 for CAT-SC and 0.909 for CAT-LC. Even more, at 550°C and 7-sec., η_{ss} became for both catalysts (Fig. 17) essentially one with η_{ss}=0.983 and η_{ss}=0.949.

Furthermore, η_{ss} was calculated, using the parameters reported in Table 7 for the "reactant conversion" model at 350°C, 400°C, 450°C, 500°C and 550°C.

Selected results are given in Figs. 18 to 20. As already described for the TOS model, the η_{ss} values from the RC model and for both CAT-LS and CAT-SC, are at 350°C significantly smaller the η_{ss} values at 550°C. The η_{ss} parameter increases consistently, however with the reactant conversion and this is in agreement with the model advanced with eq. (19). In addition, with the increasing temperature level there is a tendency for η_{ss} to reach higher values (η_{ss} close to unity). In particular at 550°C and for the two catalysts and for all conversions studied (Fig.20) the η_{ss} parameter becomes essentially unity indicating little or no diffusional constrains at the higher thermal levels. Thus, the consideration of the RC deactivation model allows to predict that η_{ss} increases with conversion, with η_{ss} values becoming close to one at 550°C. This allows postulating strong transport intra-crystal limitations at 350°C with the overall cracking reaction becoming controlled by the intrinsic kinetics at 550°C.

As a result, it can be stated that in the 350-450°C range there are significant transport constrains affecting the cracking rate of 1,3,5-TIPB. These constrains are reduced becoming essentially negligible at 500-550°C. From a fundamental point of view, these findings can be explained given the different magnitude of the expected activation energies for configurational diffusion, dominating the intracrystalline 1,3,5-TIPB transport, and for the intrinsic cracking reaction. The energy of activation for diffusion is 16 Kcal/mole and this is much larger than the 6-7 Kcal/mole for the intrinsic cracking reaction. Thus, at 350-450°C the effect of temperature is given by eq (15) and eq(19), with the overall kinetic constant displaying an apparent activation energy of 11 Kcal/mole. At 500-550°C, the modified Thiele modulus is small enough and η_{ss} becomes in all

cases, close to unity. As a result, the intra-crystal diffusional transport dominates the lower temperature operation range with the higher operating temperatures falling essentially in the chemical controlled regime.

Moreover if the extent of 1,3,5-TIPB cracking is set at a given conversion level (e.g. 40% conversion), reducing the zeolite crystal size gives, for the complete temperature range (350-550°C), η_{ss} values very close to unity (Fig 21). This demonstrates that manufacturing FCC catalyst with 0.1-μm zeolites, frees the 1,3,5-TIPB, of transport constrains. Thus, FCC catalysts manufactured with 0.1-μm crystals are highly recommended.

Conclusions

a) A set of equations involving unsteady state balances for both the gas phase and the catalyst particles, are required for modeling catalytic cracking of hydrocarbons in a Riser Simulator.

b) A quasi-steady state approximation can be adopted, under the operating conditions of the present study, for the FCC catalyst particles,

c) Activity decay models and in particular a decay model based on reactant conversion, are of important value for modelling the experimental reaction data.

d) The parameters and decay constants of these models can be assessed using non-linear regression analysis with parameters being established with adequate statistical indicators.

e) The calculated Thiele modulus and the effectiveness show the effect of crystal size and temperature on the operating regime of the catalyst,

f) Results obtained using two zeolite crystal sizes, point toward two regimes affecting the FCC catalyst operation: a) a diffusion controlled regime prevalent at the lower temperatures (350–450°C), b) a chemical controlled regime dominant at the higher temperatures (500–550°C).

Acknowledgments

The authors would like to express their appreciation to the King Fahd University of Petroleum and Minerals (KFUPM) that provided a postgraduate scholarship to Mr. S. Al-Khattaf. The authors are also very grateful for the

financial support of Venezuelan government through Fundación Gran Mariscal de Ayacucho providing a postgraduate scholarship to J. A. Atias. The authors would like to acknowledge the support of Dr A. Humphries from Akzo Nobel and of J. Macaoay from Engelhard companies, who contributed significantly to this study with the preparation of the catalysts.

Nomenclature

a_{ext} Specific external surface area for the zeolite crystal (m^2/m^3)

A Constant (-)

C_A Concentration of A species at bulk conditions. Refer to condition of eq. (4). ($kmole/m^3$)

$C_{A,in}$ Concentration of A species inside the crystals ($kmole/m^3$)

$C_{A,ex}$ Concentration of A species outside the crystals or bulk conditions ($kmole/m^3$)

$C_A\big|_{r=R_{cr}}$ Concentration of A species in the zeolite pore mouth ($kmole/m^3$)

$C_{A,ex}\big|_{\tau=0}$ Initial bulk concentration of the A chemical species. ($kmol/cm^3$)

$C^*_{A,in} = \dfrac{C_{A,in}}{C_{A,ex}\big|_{\tau=0}}$, Dimensionless internal concentration (-)

$C^*_{A,ex} = \dfrac{C_{A,ex}}{C_{A,ex}\big|_{\tau=0}}$, Dimensionless bulk concentration (-)

D_{eff} Effective diffusivity (m^2/s).

D_0 Pre-exponential constant for the diffusivity coefficient (m^2/s)

E_D Diffusion activation energy (kcal/kmole)

E_R Energy of activation for reaction (kcal/kmole)

$h = R_{cr}\sqrt{\frac{k_{A,in}\varphi_{in}\rho_{cr}}{D_{eff}}}$ Thiele modulus (-)

h' Modified Thiele modulus (-)

$k_{A,in}$ Intrinsic kinetic constant (m3 grcrystal s^{-1})

$k_0^{'}$ Intrinsic kinetic constant for the cracking of 1,3,5-TIPB defined at the reference temperature To=723 K (s^{-1})

K Adsorption constant (m^3/kg crystal)

MW_A 1,3,5-TIPB molecular weight (kg/kgmole).

MW_{coke} Coke molecular weight (kg/kgmole).

r Radial direction (m)

r_A Reaction rate at bulk conditions (kmole/kgcrystal.s)

r_{mean} Volumetric average reaction rate in the crystals (kmole/kgcrystal.s)

$r^* = \frac{r}{R_{crr}}$ Dimensionless radial distance (-)

R Universal gas constant (kcal/kmole.K)

R_{cr} Crystal radius (m^2)

t Time (sec.)

T Temperature (K)

T_0 Reference temperature of 723 K

V Riser Simulator volume (m^3)

W_c Catalyst weight (kg).

W_{cr} Weight of crystal (kg)

W_{hc} Total mass of hydrocarbons injected in the riser (kg)

X_{coke} Coke mass fraction based on the catalyst weight (-)

y_A 1,3,5-TIPB mass fraction (-)

Greek Symbols

α Constant (s^{-1})

δ Constant (-)

ε Crystal voidage (m^3 void in crystal / m^3 crystal)

φ_{in} Intrinsic catalyst activity decay function (-)

λ Constant (-)

η Effectiveness factor (-)

η_{ss} Effectiveness factor at steady state (-)

ρ_{cr} Density of the crystal (kg crystal /m^3)

$\tau = \frac{D_{eff} t}{R_{cr}^2 (\varepsilon + K\rho_c)}$ Dimensionless time (-)

ν_{coke} Stoichiometric coefficient for the formation of coke from the 1,3,5-TIPB cracking (-)

References

Al-Khattaf, S. (2001). Diffusion and Reaction of Hydrocarbons in FCC Catalysts, Ph.D Dissertation, University of Western Ontario, London, Ontario, Canada.

S.Al-Khattaf, S. & de Lasa, H. (2001a). The Role of Diffusion in Alkyl-benzenes Catalytic Cracking. Submitted Applied Catalysis.

Al-Khattaf, S & de Lasa, H. (2001b). Catalytic Cracking of 1,3,5 Tri-iso-propyl-benzene in a Novel CREC Riser Simulator. Stu.Surf.Sci.Catal., 134, 279-287.

Al-Khattaf, S. & de Lasa, H. (2001c). Diffusion and Reactivity of Hydrocarbon Feedstocks in FCC Catalysts, in press Can.J.Chem.Engng.

Al-Khattaf, S & de Lasa, H. (2000a). Catalytic Cracking of Cumene in a Riser Simulator. A catalyst activity decay model. Submitted Ind.Engng.Chem.Res.

Al-Khataff, S & de Lasa, H. (1999). Activity and Selectivity of FCC Catalysts in a Riser Simulator. The Role of Y-zeolite. Ind.Engng.Chem.Res., 38, 1350-1356.

Aguiar, E. F., Murta Valle, M. L., Silva, M. P. & Silva, D. F. (1995). Influence of External Surface Area of Rare-Earth Containing Y Zeolites on the Cracking of 1,3,5-Triisopropylbenzene". Zeolites, 15, 620-623.

Arandes, J.M., Abajo, I., Fernandez, I., Azkoiti, M.J. & Bilbao, J. (2000). Effect of HZSM-5 Zeolite Addition to a Fluid Catalytic Cracking Catalyst. Study in a Laboratory Reactor Operating under Industrial Conditions. Ind. Eng. Chem. Res., 39, 1917-1924.

Arandes, J.M., Abajo, I., Lopez-Valerio, D., Fernandez, I., Azkoiti, M. J., Olazar, M. & Bilbao, J. (1997). Transformation of Several Plastic Wastes into Fuels by Catalytic Cracking, Ind. Eng. Chem. Res., 36, 4523-4529.

Aris, R. (1969). Elementary Chemical Reactor Analysis, First edition, Prentice Hall.

Bhatai, S. (1990). Zeolite Catalysts, Principles and Applications", CRC Press, Boca Ration, 7-18, 239-250.

Bidabehere, C.M. & Sedran, U. (2000). Simultaneous Diffusion, Adsorption, and Reaction in Fluid Catalytic Cracking Catalysts. Ind. Eng. Chem. Res., 40, 530-535.

Corma, A., & Wojciechowski, B.,W. (1982). The Catalytic Cracking of Cumene. Cat. Rev. Sci. Eng., 24 (1), 1-65.

de Lasa, H.I., (1991). Riser Simulator for Catalytic Cracking Studies. U.S. Patent #5,102,628.

Froment, G. F. & Bischoff, K. B. (1979). Chemical Reactor Analysis and Design", Second Edition, J.Wiley.

Gates, B.C., Katzer, J.R. & Schuit, G.C. (1979). Chemistry of catalytic processes. McGraw-Hill Inc.

Haag, W.O., Lago, R.M. & Weisz, P.B. (1982). Transport and reactivity of hydrocarbon molecules in a shape-selective zeolite. Faraday Discuss. 72 317

Karger,J., & Ruthven, D.M. (1992). Diffusion in Zeolites and Other Microporous Solids. John Wiley & Sons, Inc.

Leiby, S. (1992). FCC Catalyst Technologies Expand Limits of Process Capability", Oil & Gas Journal, March 23rd, 49-58.

Levenspiel, O. (1972). Chemical Reaction Engineering, Second edition., John Wiley, New York.

Pruski, J. (1996). Catalytic Cracking of Hydrocarbons in a Novel Riser Simulator: Adsorption Phenomena; M.E.Sc. Thesis Dissertation, University of Western Ontario, London, Canada.

Roos, K., Liepold, A., Koch, H., & Reschetilowski, W. (1997). Impact of Accessibility and Acidity on Novel Molecular Sieves for Catalytic Cracking of Hydrocarbons. Chemical Engineering Technology, 20, 326-332.

Ruthven, D.M. & Kaul, B.K. (1993). Adsorption of Aromatic Hydrocarbons in NaX Zeolite. 2.Kinetics. Ind. Eng. Chem. Res., 32, 538-541.

Sedran, U. (1994). Laboratory Testing of FCC Catalysts and Hydrogen Transfer Properties Evaluation. Catal. Rev. Sci. Eng., 36, 405-431.

Tsai, T., Liu, S., & Wang, I. (1999). Disproportionation and Transalkylation of Alkylbenzenes over Zeolite Catalysts. Applied Catalysis A, 181, 181-355.

Venuto, P.B., Habib, E.T. (1979). Fluid Catalytic Cracking with Zeolite Catalysts. Marcel Dekker, New York.

Venuto, P.B. & Habib, E.T. (1979). Fluid Catalytic Cracking with Zeolite Catalysts. New York, NY: Marcel Dekker.

Voorhies, A. (1945). Carbon formation in catalytic crackin., Ind. Eng. Chem., 37(4), 318-322.

Smith. J.M. (1981). Chemical Engineering Kinetics. McGraw-Hill, N.Y.

Figure Captions

Figure 1. Configuration of an FCC catalyst pellet showing: a) the pellet (macroparticle) with a dimension close to 60 μm, b) the dispersed zeolite crystals (microparticles), c) the zeolite faujasite structure.

Figure 2. Changes of the dimensionless concentration with radial position inside the Y zeolite crystals between 0 and 10 sec. of reaction time. T= 350°C.

Figure 3a. Changes of the effectiveness factor with reaction time.

Full line represents the calculated η values with eq(3) and the dimensionless concentration profiles given by eq(2).

Broken line represents the calculated η_{ss} using the quasi-steady state approximation with the accumulation term of eq. (3) neglected.

Figure 3b Changes of the deviation (%) with reaction time.

Deviation is defined on a percentual basis with the difference between predictions of the η with eqs (1) and (2) and the η_{ss} calculated with eqs(1) and the simplified eq(2) (no accumulation term)

Figure 4. Schematic representation of CREC Riser Simulator.

Figure 5. Schematic diagram of the Riser Simulator experimental setup and accessories.

Figure 6. Schematic description of the catalytic cracking of 1,3,5-TIPB.

Figure 7 1,3,5-TIPB cracking. Effect of temperature and Y-zeolite crystal size on 1,3,5-TIPB conversion. Reaction time =3 sec., C/O =5, (●) CAT-SC, (▲) CAT-LC. Reported experimental points are average values of at least 3 measurements. Typical errors are ± 2%.

Figure 8. 1,3,5-TIPB cracking. Effect of temperature and Y-zeolite crystal size on 1,3,5-TIPB conversion. Reaction time =5 sec., C/O =5, (●) CAT-SC, (▲) CAT-LC. Reported experimental points are average values of at least 3 measurements. Typical errors are ± 2%.

Figure 9a Comparison between experimental data and RC model for the 1,3,5-TIPB conversion (CAT-LC).

Figure 9b. Comparison between experimental data and RC model for the 1,3,5-TIPB conversion (CAT-LC).

Figure 10a. Comparison between experimental data and RC model for the 1,3,5-TIPB conversion (CAT-LC).

Figure 10b. Comparison between experimental data and RC model for the 1,3,5-TIPB conversion (CAT-SC).

Figure 11. 1,3,5-TIPB conversion versus reaction time using RC model for CAT-LC, C/O=5.

Figure 12. 1,3,5-TIPB conversion versus reaction time using RC model for CAT-SC, C/O=5.

Figure 13. Coke selectivity for 1,3,5-TIPB conversion versus reaction time. C/O=5, CAT-LC, (●) T=400°C, (■) T=450°C.

Figure 14. Coke selectivity for 1,3 5,-TIPB conversion versus reaction time. C/O=5, CAT-LC, (■) T=500°C, (△) T=550°C.

Figure 15. Effectiveness factor for the 1,3,5-TIPB conversion versus modified Thiele modulus (TOS model) for different reaction times. T=350°C, C/O=5, (□) CAT-SC, (△) CAT-LC.

Figure 16. The effectiveness factor for the 1,3,5-TIPB conversion versus modified Thiele modulus (TOS model) for different reaction times. T=450°C, C/O=5, (□) CAT-SC, (△) CAT-LC.

Figure 17. Effectiveness factor for 1,3,5-TIPB conversion versus modified Thiele modulus (TOS model) for different reaction times. T=550°C, C/O=5. (□) CAT-SC, (△) CAT-LC.

Figure 18. Effectiveness factor for 1,3,5-TIPB conversion versus modified Thiele modulus (RC model) for different reaction times. T=350°C, C/O=5. (□) CAT-SC, (△)CAT-LC.

Figure 19. Effectiveness factor for 1,3,5-TIPB conversion versus modified Thiele modulus (RC model) for different reaction time. T=450°C, C/O=5. (□) CAT-SC, (△) CAT-LC.

Figure 20. Effectiveness factor for 1,3,5-TIPB conversion versus modified Thiele modulus (RC model) for different reaction times. T=550°C, C/O=5. (□) CAT-SC, (△) CAT-LC.

Figure 21. The effect of zeolite crystal size on the effectiveness factor (RC-model). Conversion of 1,3,5-TIPB: 0.4

Parameter	Value
K (m^3 /kg crystal)	$11.82.10^{-3}$
ε (m^3 void in crystal / m^3 crystal)	0.51
ρ_c (kg crystal /m^3)	825
R_{cr} (m)	$0.45.10^{-6}$
h' at 350°C	5.1
h' for other temperatures	eq(20)
φ_{in}	$\exp(-\alpha t)$
α	Table 4
D_{eff} (m^2 / s)	eq (21)

Table 1. Adsorption, reaction and zeolite crystal parameters used in the simulation reported in Figures 2, 3a and 3b.

	CAT-SC, Catalyst with small zeolite crystals	CAT-LC, Catalyst with large zeolite crystals
Na_2O (wt%)	4.1	0.25
SiO_2/Al_2O_3 (mol/mol)	5.6	5.7
Unit cell size (Å)	24.49	24.51
Crystal size (μm)	0.4	0.9

Table 2. Properties of the catalyst with small zeolite crystals (CAT-SC) and of the catalyst with large zeolite crystals (CAT-LC).

	CAT-SC, Catalyst with small zeolite crystals	CAT-LC, Catalyst with large zeolite crystals
Unit cell size (Å)	24.28	24.28
BET Surface Area (m^2/g)	148	155
Na_2O (wt%)	Negligible	Negligible
Crystal Size (μm)	0.4	0.9

Table 3. Properties of the catalyst with small zeolite crystals (CAT-SC) and of the catalyst with large zeolite crystal (CAT-LC).

Catalyst	$k'_0 10^3$ (m^3/kg-crystal.sec)	95% CFL	E_R (kcal/mol)	95% CFL	α (1/sec)	95% CFL
CAT-LC	52.7	12.3	0.905	1.37	0.205	0.071
CAT-SC	40.34	8.83	2.64	1.08	0.220	0.078

Table 4. Kinetic constants for both CAT-SC and CAT-LC based on time on stream (TOS)

k'_0	1	-0.41	0.927
E_R	-0.41	1	-0.177
α	0.927	-0.177	1

Table 5. Correlation matrix for CAT-LC (TOS-model)

k'_0	1	-0.35	0.951
E_R	-0.35	1	-0.211
α	0.951	-0.21	1

Table 6. Correlation matrix for CAT-SC (TOS-model)

Catalyst	$k'_0 10^3$ (m^3/kg-crystal.sec)	95% CFL	E_R (kcal/mole)	95% CFL	λ	95% CFL
CAT-LC	66.183	28.5	6.19	2.94	3.69	1.58
CAT-SC	59.123	31.5	7.19	2.67	3.841	1.76

Table 7. Kinetic constants for both CAT-SC and CAT-LC based on reactant conversion (RC).

k'_0	1	0.589	0.954
E_R	0.589	1	0.731
λ	0.954	0.731	1

Table 8 Correlation matrix for CAT-LC (RC-model).

k'_0	1	0.660	0.974
E_R	0.660	1	0.727
λ	0.974	0.727	1

Table 9. Correlation matrix for CAT-SC (RC-model).

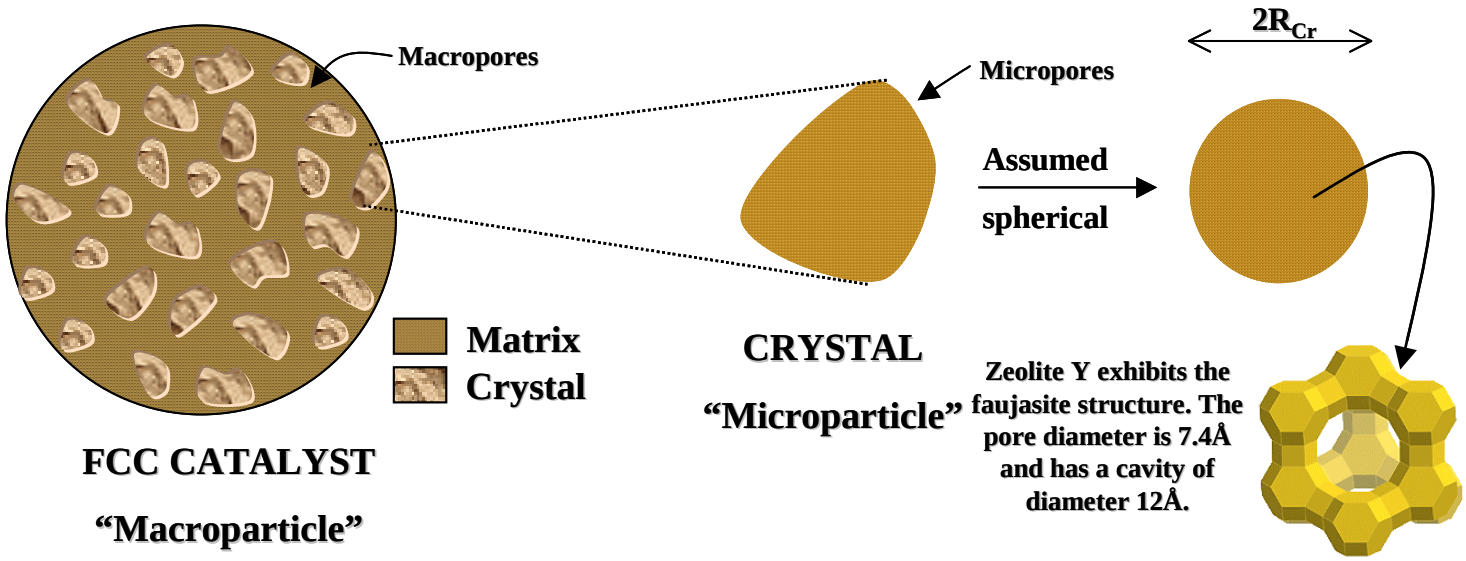

Figure 1. Configuration of an FCC catalyst pellet showing:
a) the pellet (macroparticle) with a dimension close to 60-μm,
b) the dispersed zeolite crystals (microparticles), c) the zeolite faujasite structure.

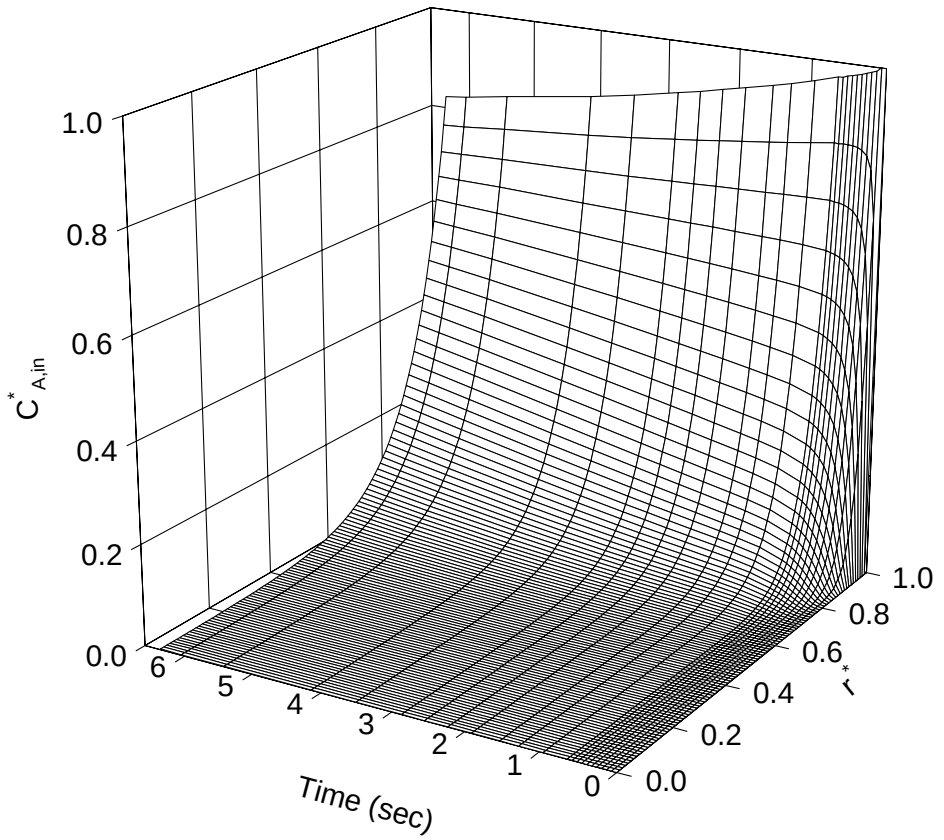

Figure 2. Changes of the dimensionless concentration with radial position inside the Y zeolite crystals between 0 and 6-sec. of reaction time. T= 350°C.

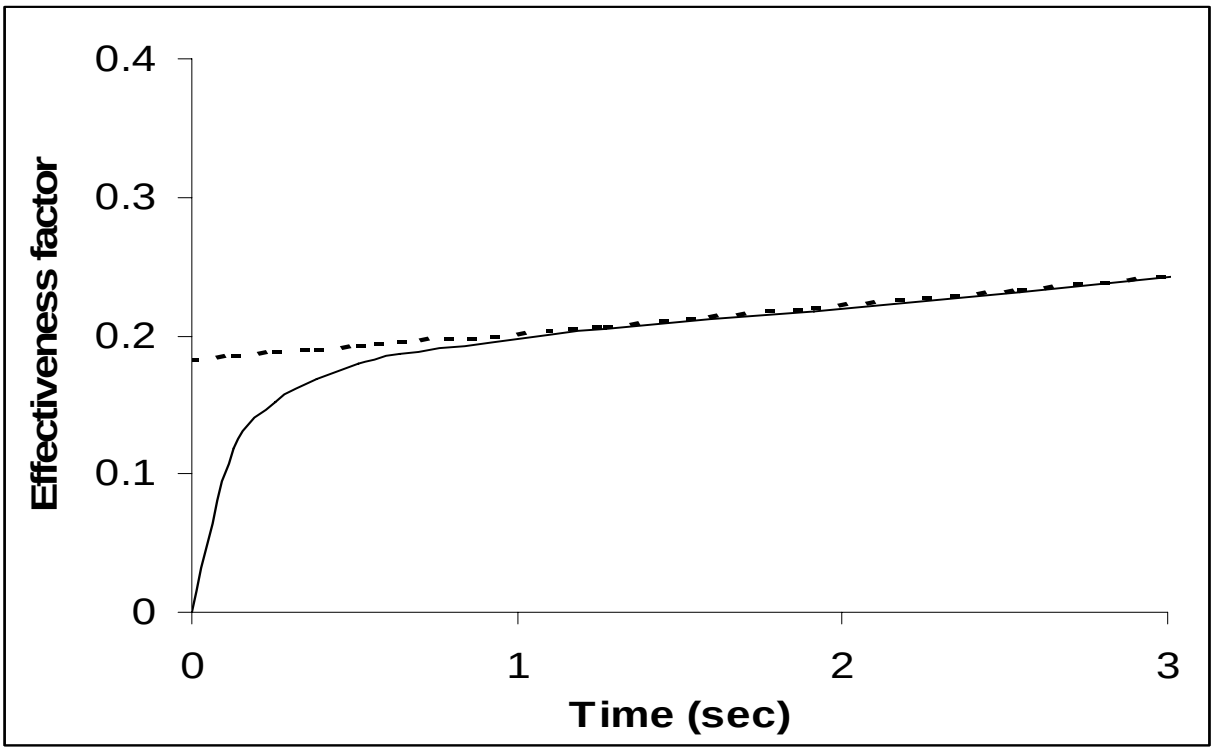

Figure 3a. Changes of the effectiveness factor with reaction time.
Full line represents the calculated η values with eq(3) and the dimensionless concentration profiles given by eq(2). Broken line represents the calculated η_{ss} using the quasi-steady state approximation with the accumulation term of eq. (3) neglected.

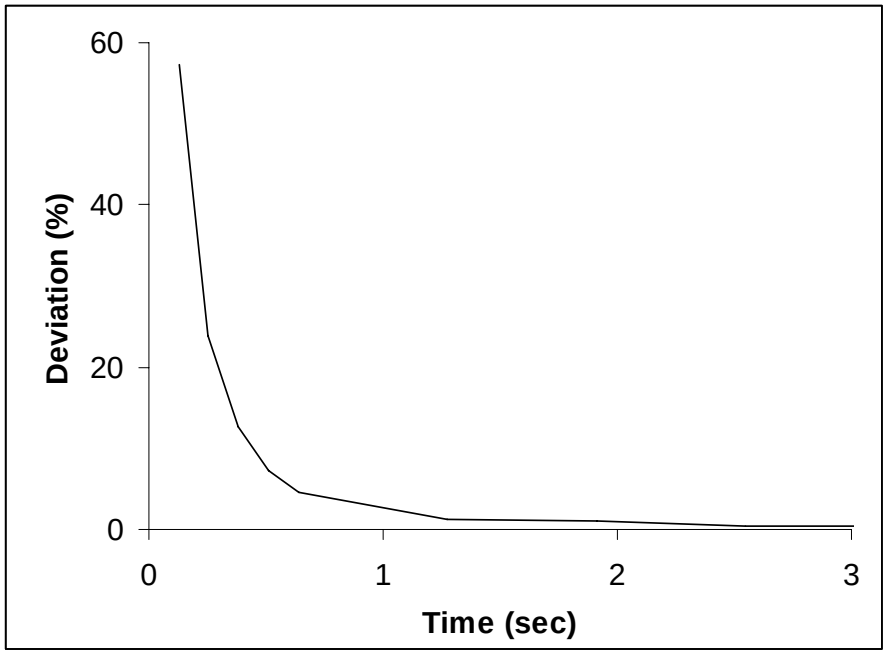

Figure 3b. Changes of the deviation (%) with reaction time.
Deviation is defined on a percentual basis with the difference between predictions of the η with eqs (1) and (2) and the η_{ss} calculated with eqs(1) and the simplified eq(2) (no accumulation term)

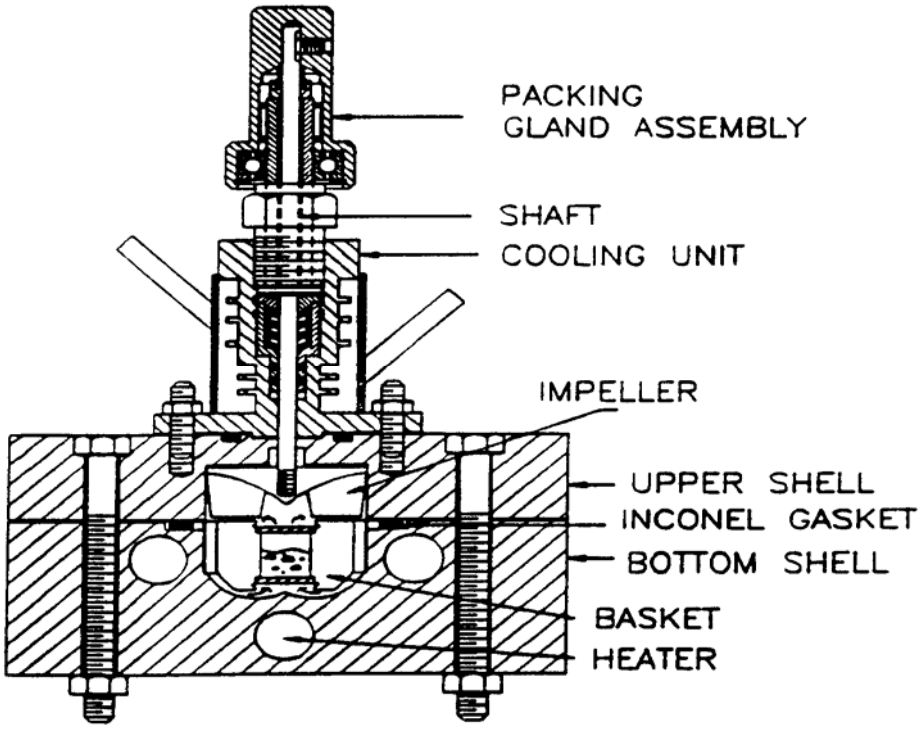

Figure 4. Schematic representation of CREC Riser Simulator.

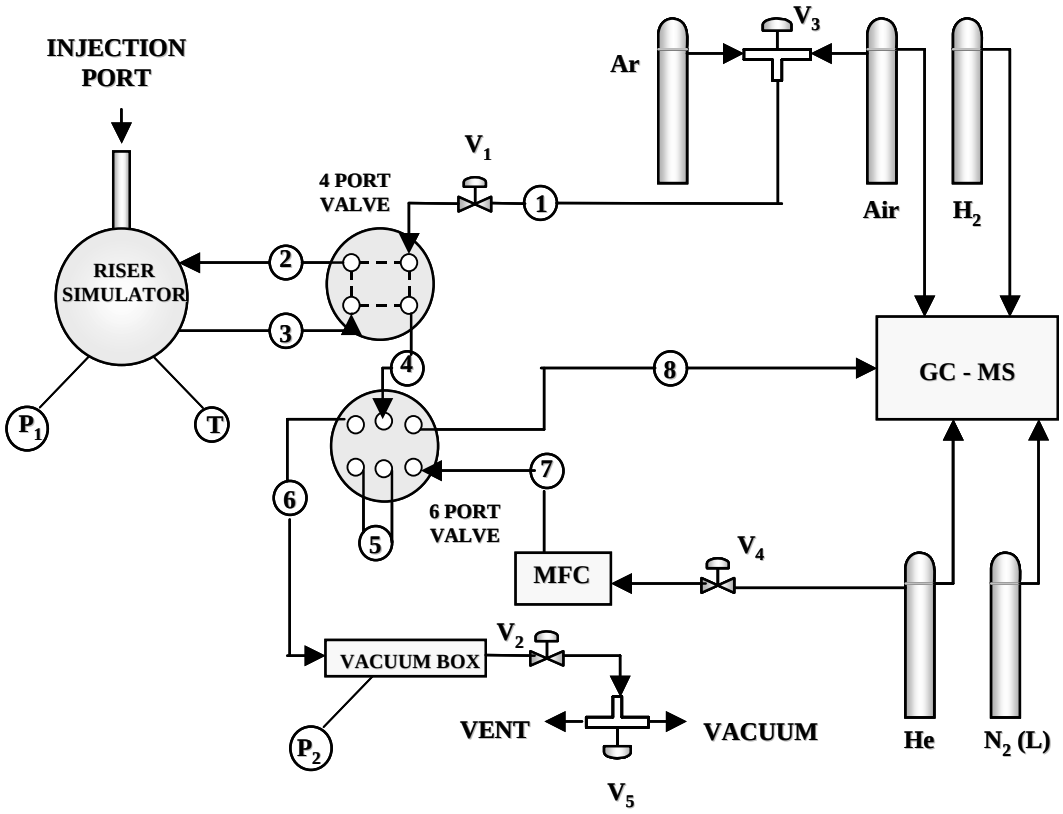

Figure 5. Schematic diagram of the Riser Simulator experimental setup and accessories.

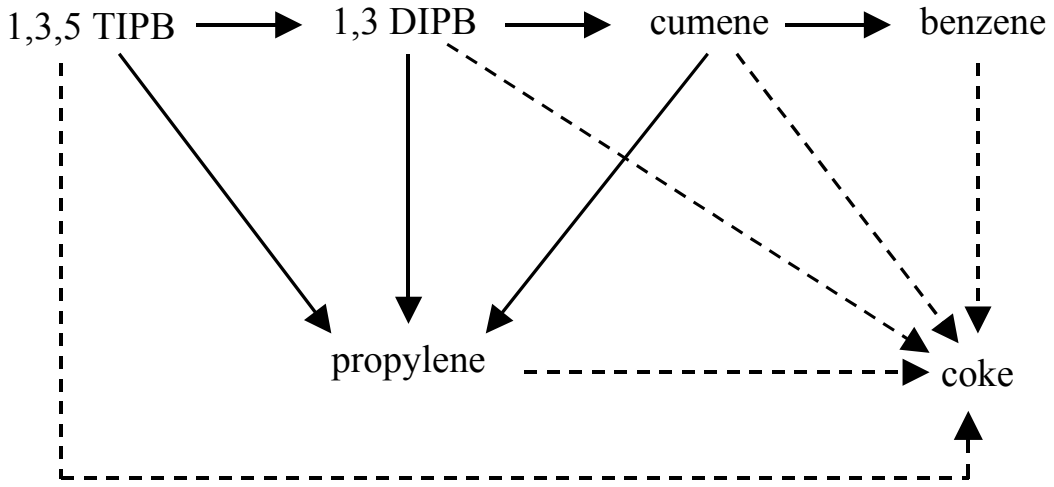

Figure 6. Schematic description of the catalytic cracking of 1,3,5-TIPB.

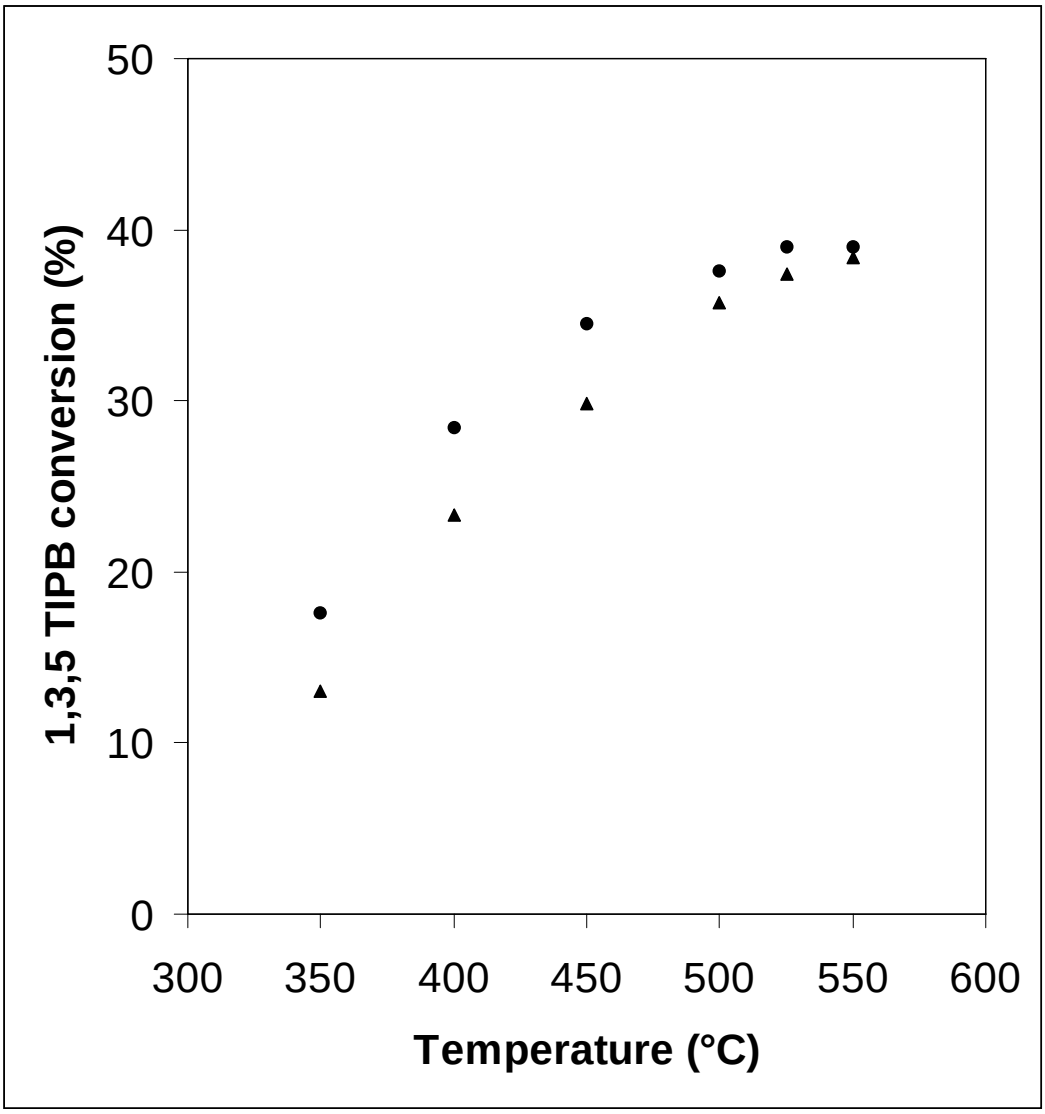

Figure 7. 1,3,5-TIPB cracking. Effect of temperature and Y-zeolite crystal size on 1,3,5-TIPB conversion. Reaction time =3 sec., C/O =5, (●) CAT-SC, (▲) CAT-LC. Reported experimental points are average values of at least 3 measurements. Typical errors are ± 2%.

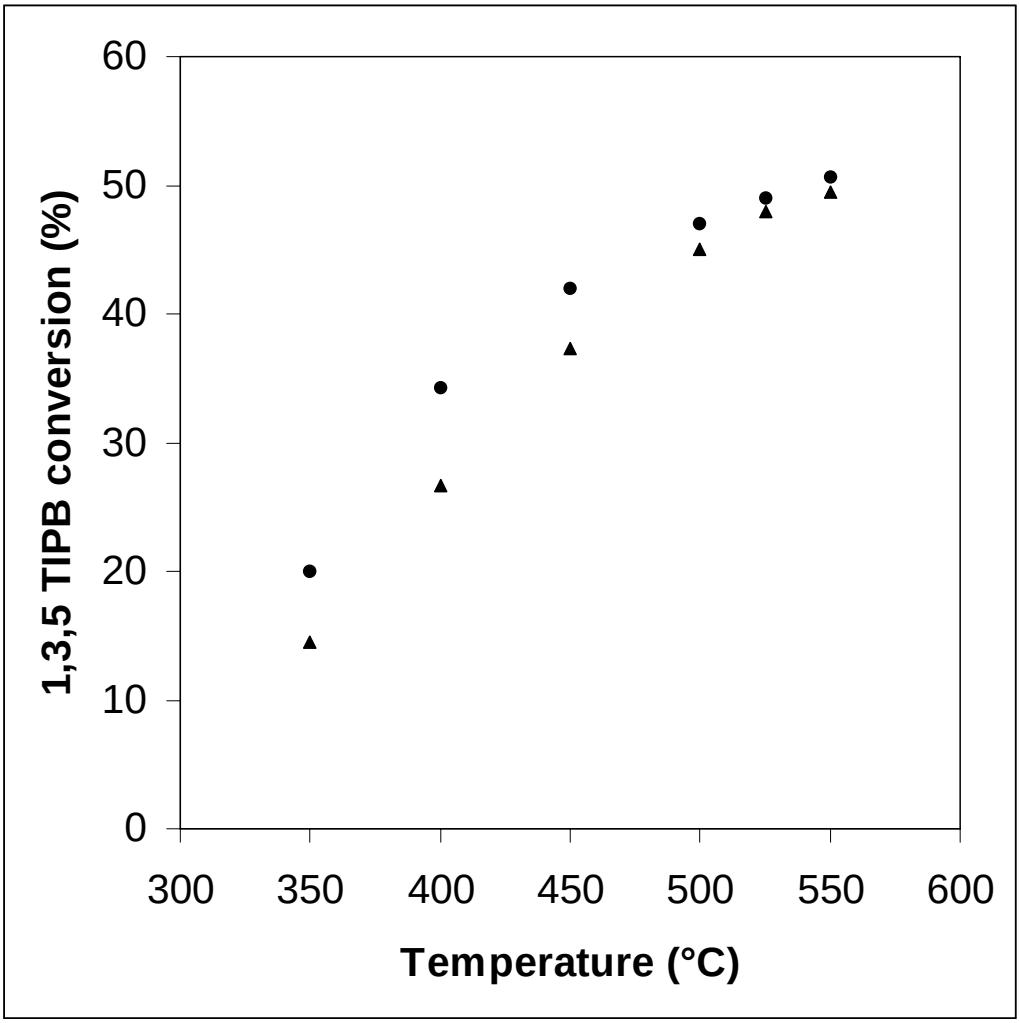

Figure 8. 1,3,5-TIPB cracking. Effect of temperature and Y-zeolite crystal size on 1,3,5-TIPB conversion. Reaction time =5 sec., C/O =5, (●) CAT-SC, (▲) CAT-LC. Reported experimental points are average values of at least 3 measurements. Typical errors are ± 2%.

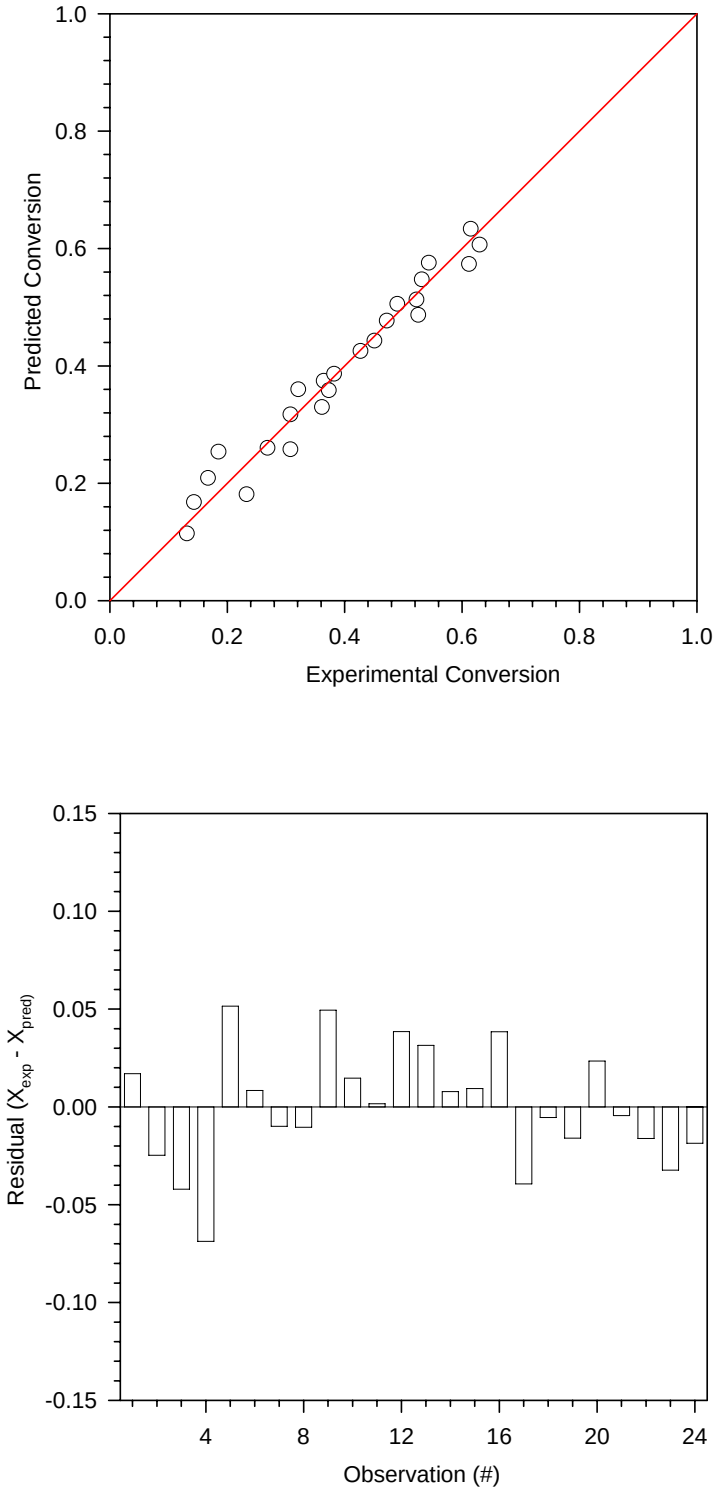

Figure 9a. Comparison between experimental data and TOS model for the 1,3,5-TIPB conversion (CAT-LC).

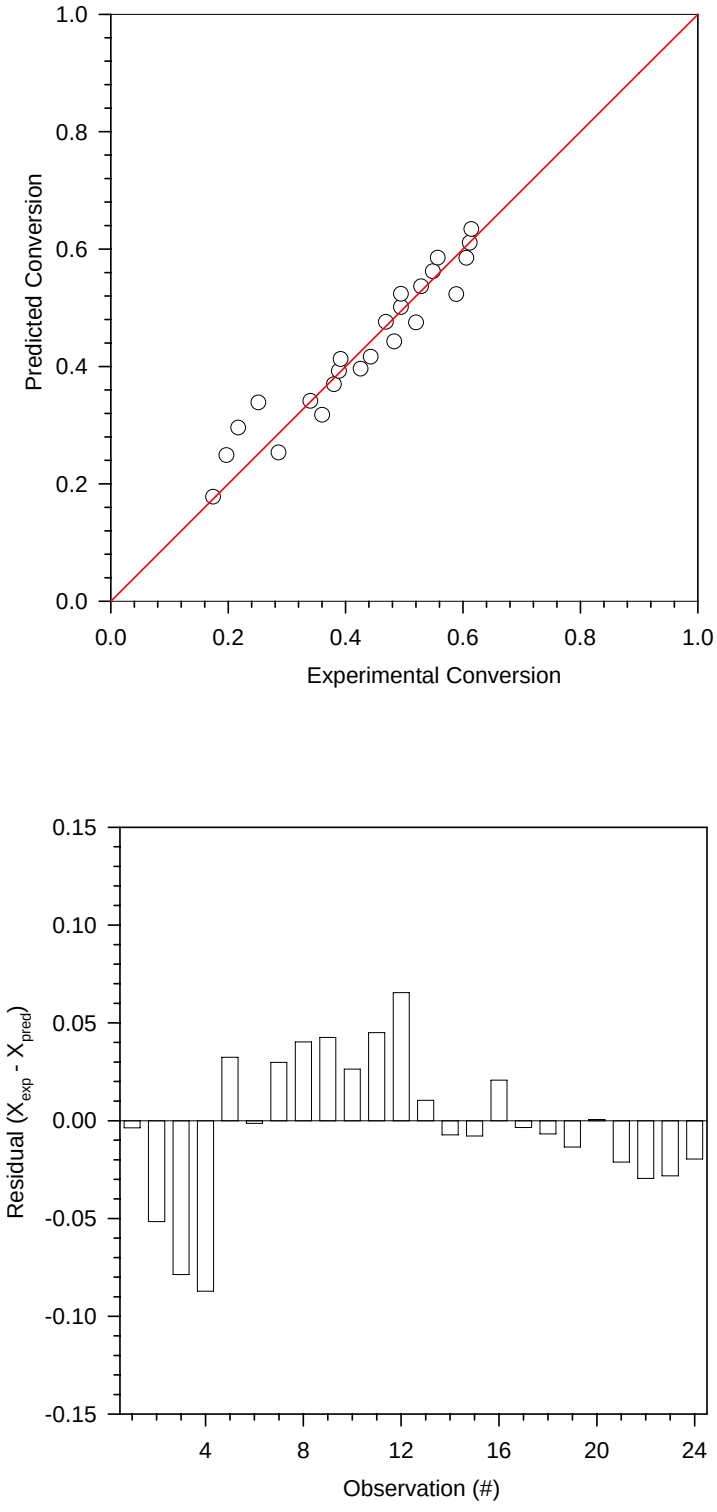

Figure 9b. Comparison between experimental data and TOS model for the 1,3,5-TIPB conversion (CAT-LC).

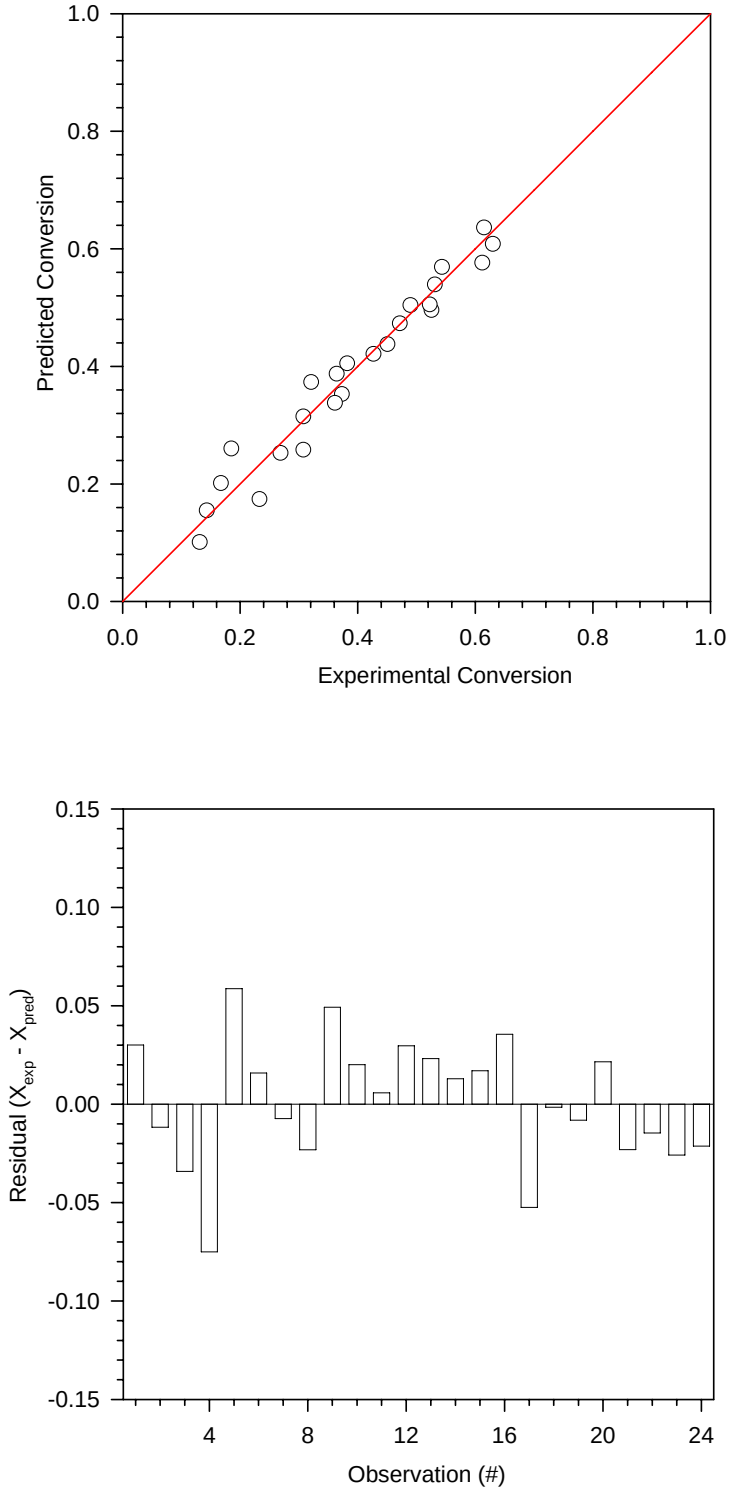

Figure 10a. Comparison between experimental data and RC model for the 1,3,5-TIPB conversion (CAT-LC).

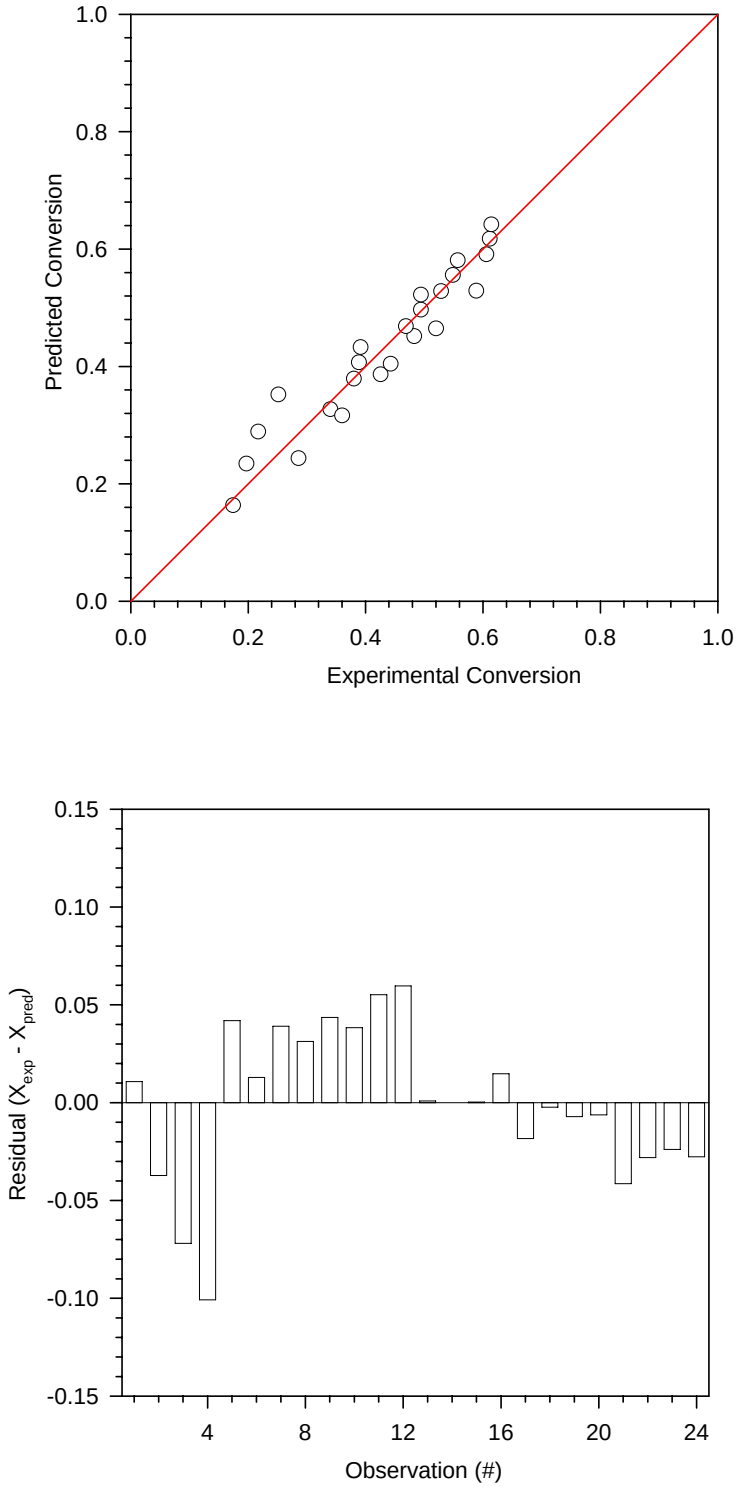

Figure 10b. Comparison between experimental data and RC model for the 1,3,5-TIPB conversion (CAT-SC).

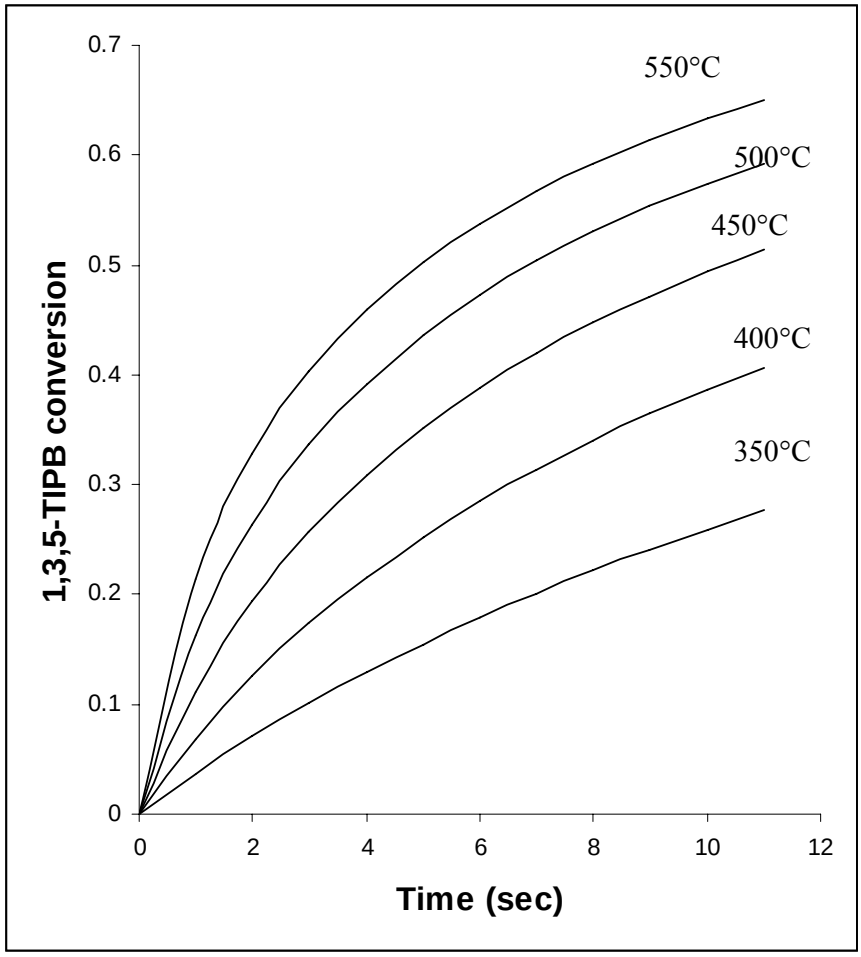

Figure 11. 1,3,5-TIPB conversion versus reaction time using RC model for CAT-LC, C/O=5.

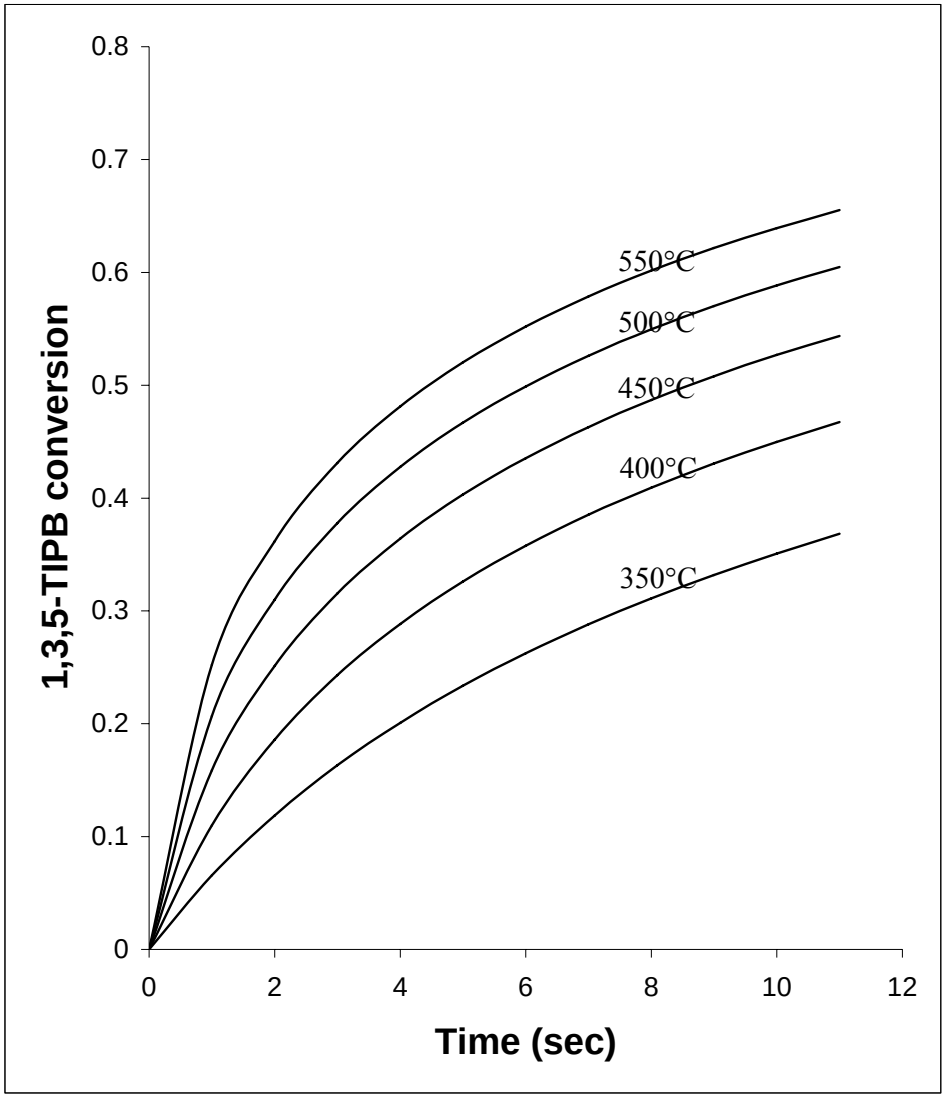

Figure 12. 1,3,5-TIPB conversion versus reaction time using RC model for CAT-SC, C/O=5.

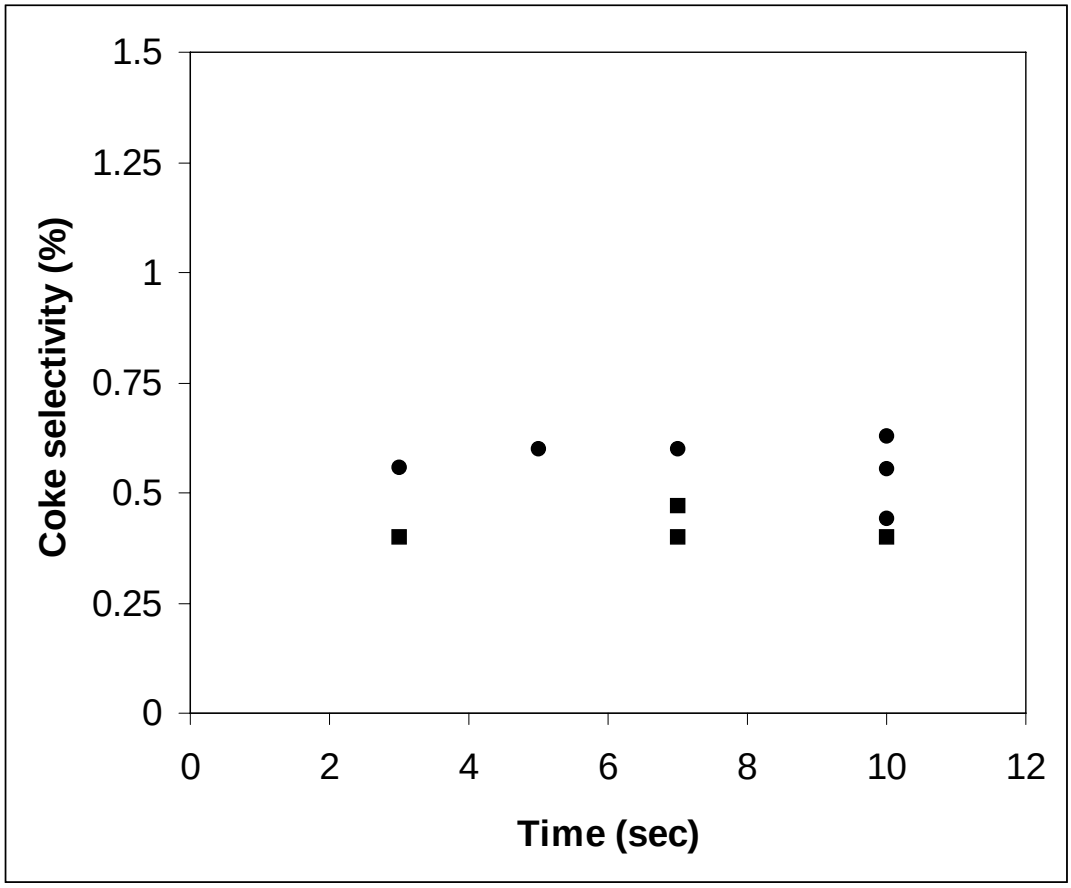

Figure 13. Coke selectivity for 1,3,5-TIPB conversion versus reaction time. C/O=5, CAT-LC, (●) T=400°C, (■) T=450°C.

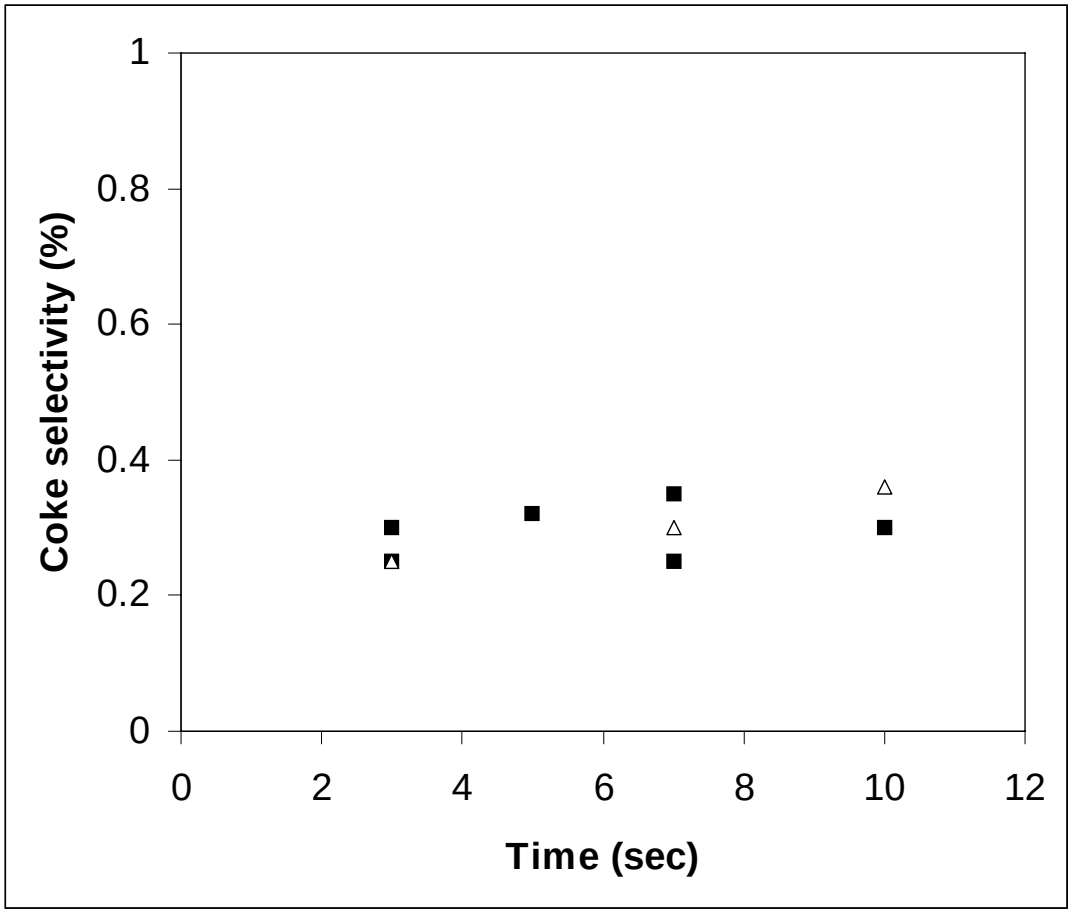

Figure 14. Coke selectivity for 1,3 5,-TIPB conversion versus reaction time. C/O=5, CAT-LC, (■) T=500°C, (△) T=550°C.

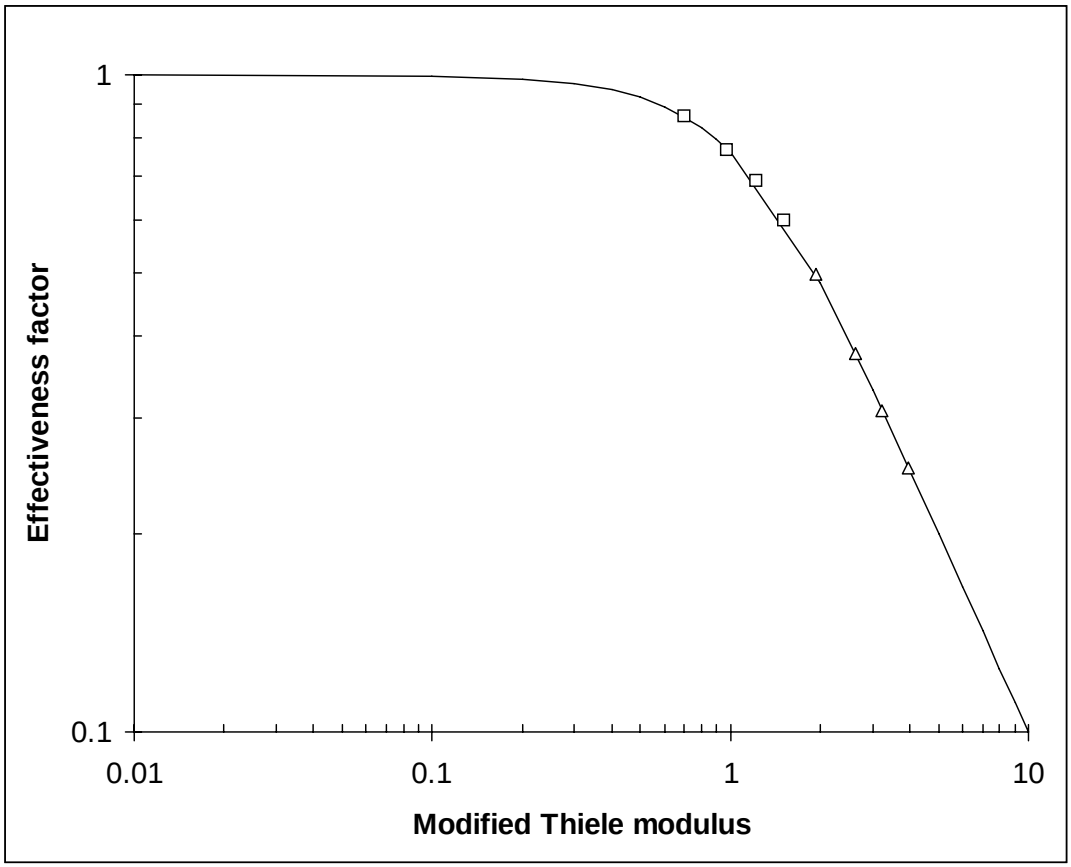

Figure 15. Effectiveness factor for the 1,3,5-TIPB conversion versus modified Thiele modulus (TOS model) for different reaction times. T=350°C, C/O=5, (□) CAT-SC, (△) CAT-LC.

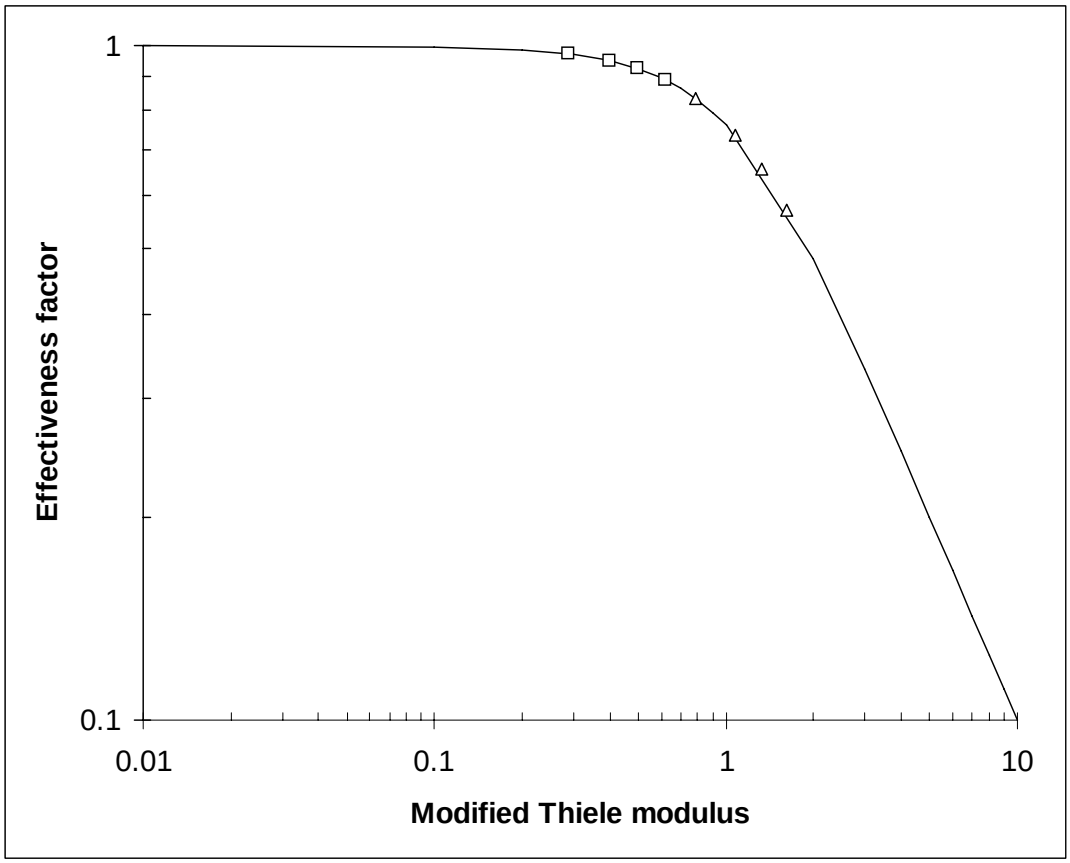

Figure 16. The effectiveness factor for the 1,3,5-TIPB conversion versus modified Thiele modulus (TOS model) for different reaction times. T=450°C, C/O=5, (□) CAT-SC, (△) CAT-LC

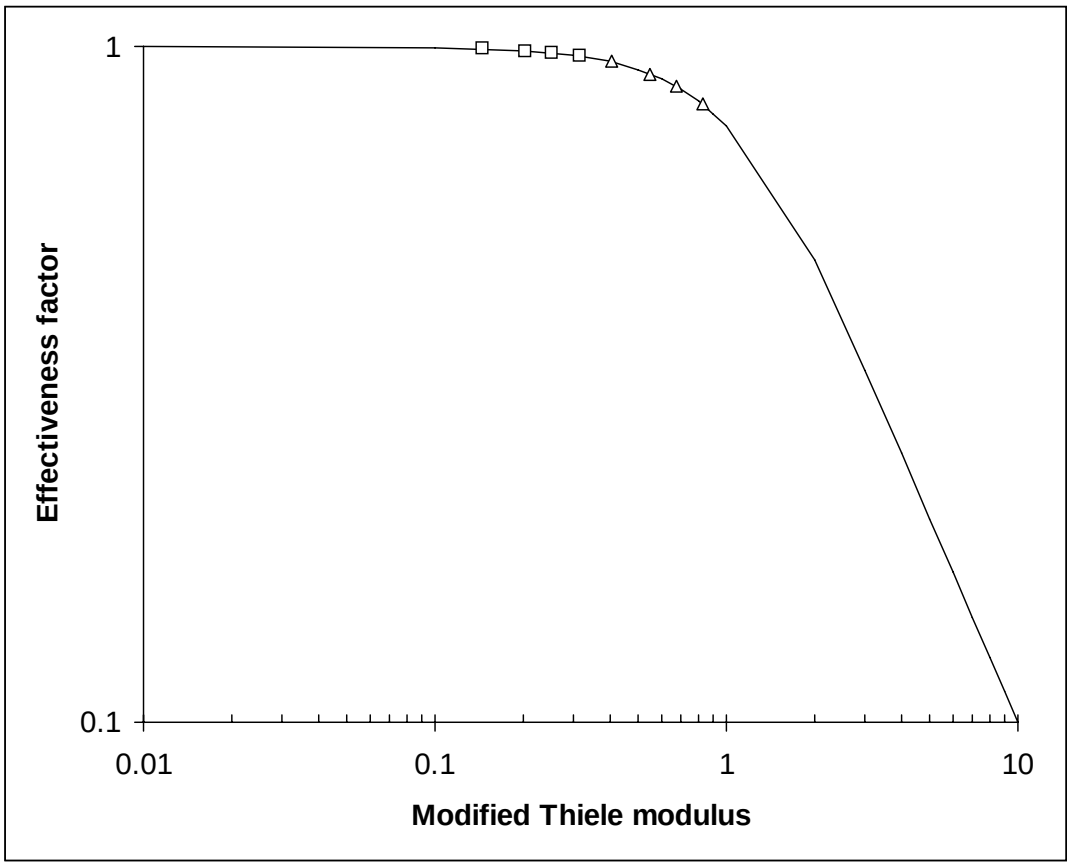

Figure 17. Effectiveness factor for 1,3,5-TIPB conversion versus modified Thiele modulus (TOS model) for different reaction times. T=550°C, C/O=5. (□) CAT-SC, (△) CAT-LC.

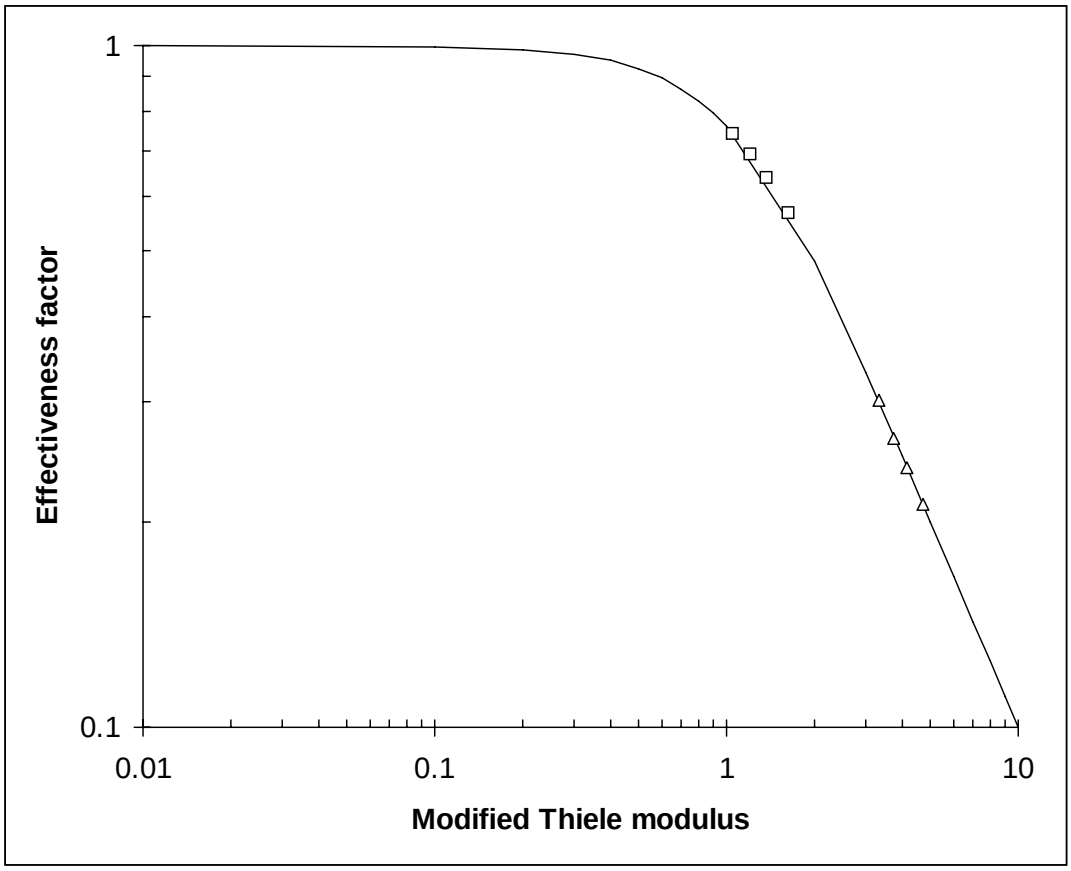

Figure 18. Effectiveness factor for 1,3,5-TIPB conversion versus modified Thiele modulus (RC model) for different reaction times. T=350°C, C/O=5. (□) CAT-SC, (△)CAT-LC.

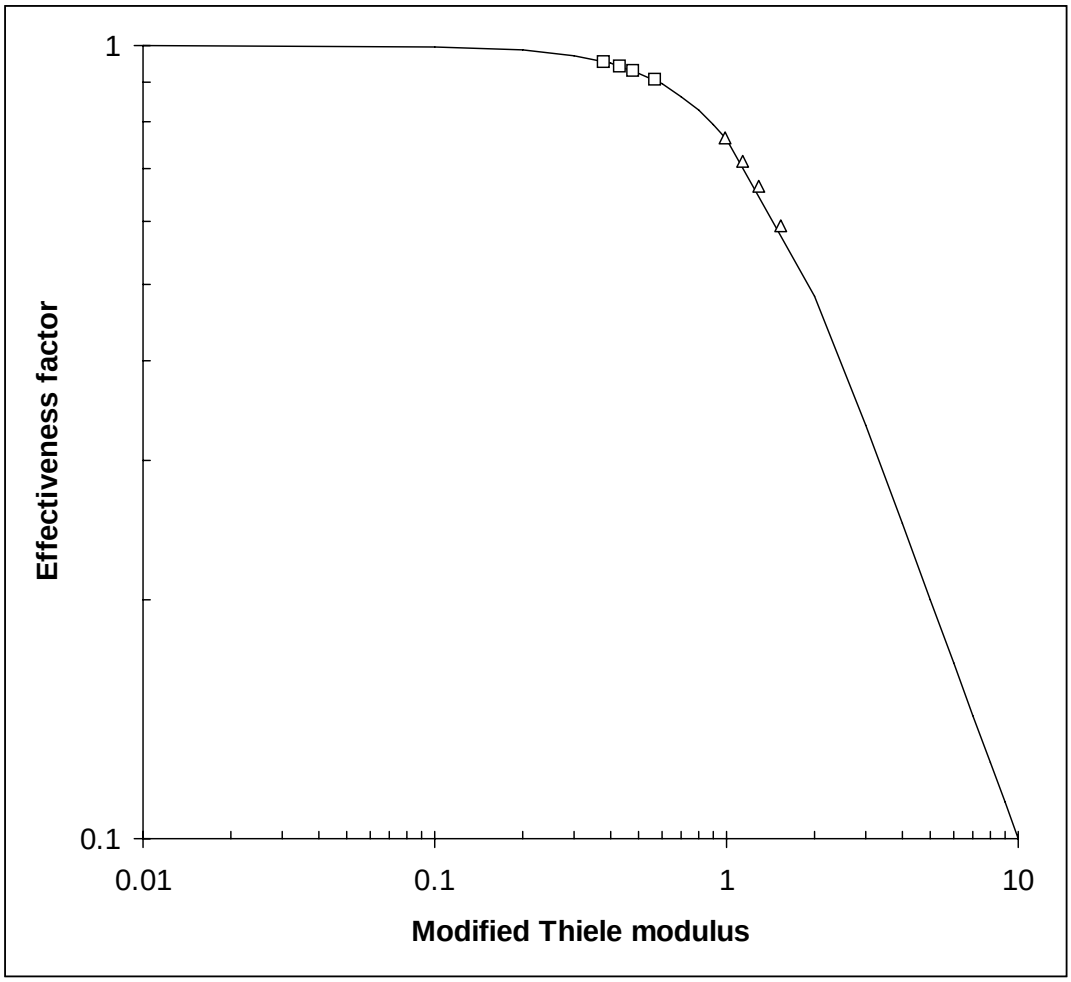

Figure 19. Effectiveness factor for 1,3,5-TIPB conversion versus modified Thiele modulus (RC model) for different reaction time. T=450°C, C/O=5. (□) CAT-SC, (△) CAT-LC.

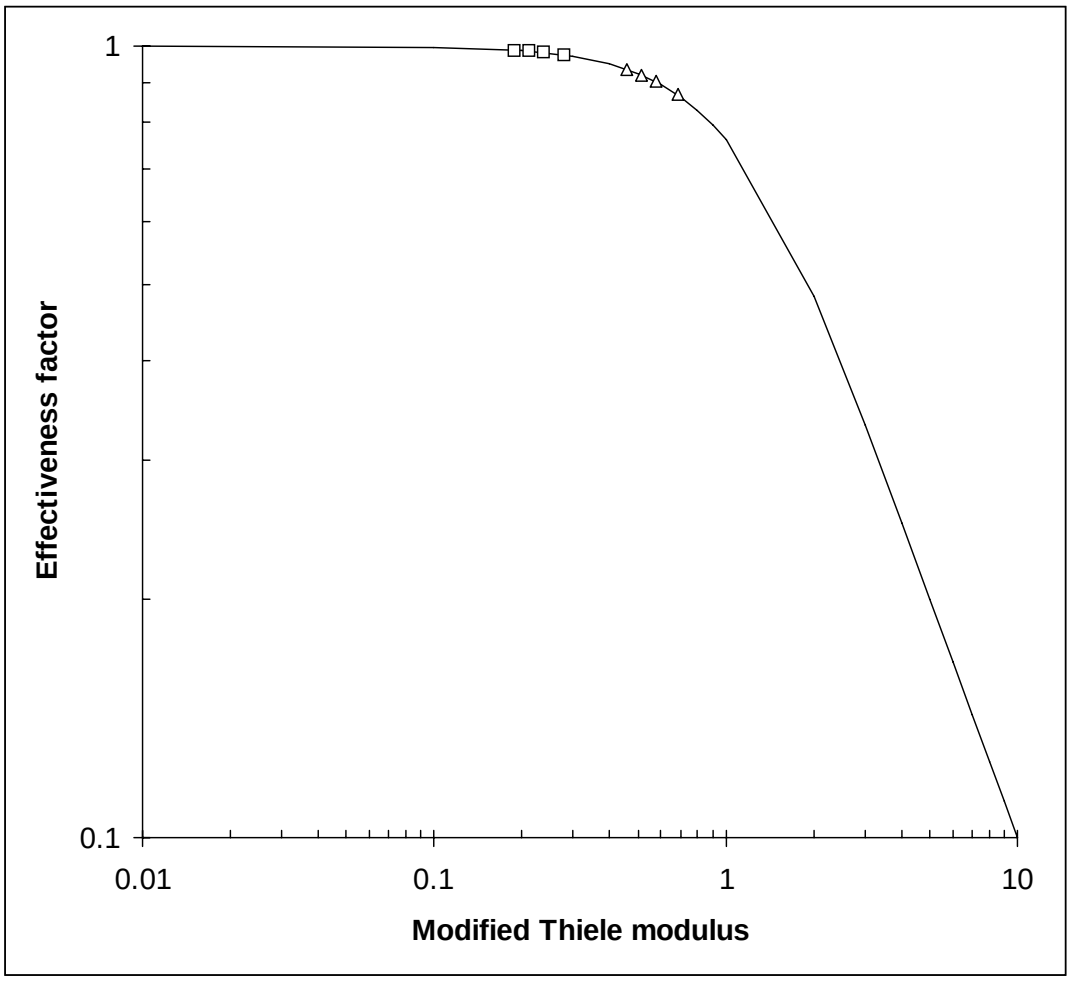

Figure 20. Effectiveness factor for 1,3,5-TIPB conversion versus modified Thiele modulus (RC model) for different reaction times. T=550°C, C/O=5. (□) CAT-SC, (△) CAT-LC.

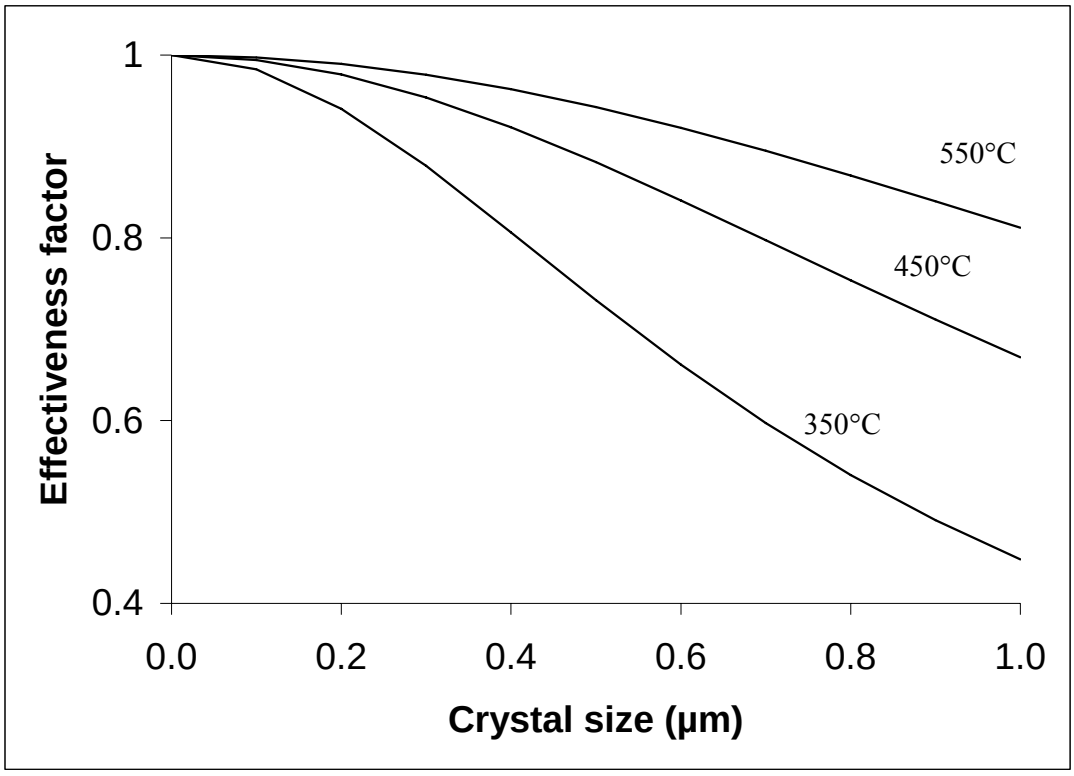

Figure 21. Effect of the zeolite crystal size on the effectiveness factor (RC-model). Conversion of 1,3,5-TIPB: 0.4 , k'_0 = 64 m^3/kg-crystal.sec , E_R = 6.5 kcal/mole), λ = 3.75